Testing fast photochemical theory during TRACE-P based on measurements of NO_2, OH, HO_2, and CH_2O

Jennifer R. Olson[1], J.H. Crawford[1], G. Chen[1], A. Fried[2], M.J. Evans[3], C.E. Jordan[1], S.T. Sandholm[4], D.D. Davis[4],B.E. Anderson[1], M.A. Avery[1], J.D. Barrick[1], D.R. Blake[5], W.H. Brune[6], F.L. Eisele[2], F. Flocke[2], H. Harder[6,7], D.J. Jacob[3], Y. Kondo[8], B.L. Lefer[2], M. Martinez[6,7], R.L. Mauldin[2], G.W. Sachse[1], R.E. Shetter[2], H.B. Singh[9], R.W. Talbot[10], D. Tan[4]

Submitted to Journal of Geophysical Research - Atmospheres
TRACE-P Second special section
October 22, 2003

[1] Atmospheric Sciences Division, Langley Research Center, NASA, Hampton, VA 23681
[2] Atmospheric Chemistry Division, National Center for Atmospheric Research, Boulder, CO
[3] Division of Engineering and Applied Science, Harvard University, Cambridge, MA
[4] School of Earth and Atmospheric Sciences, Georgia Institute of Technology, Atlanta, Georgia
[5] Department of Earth System Science, University of California-Irvine, Irvine, CA
[6] Department of Meteorology, Pennsylvania State University, University Park, PA
[7] Currently at Max Planck Institute for Chem., Mainz, Germany
[8] Solar-Terrestrial Environmental Laboratory, Nagoya University, Toyokawa, Japan
[9] Earth Science Division, NASA Ames Research Center, Moffett, CA
[10] University of New Hampshire, Durham, NH

Measurements of several key short-lived photochemical species (e.g., NO_2, OH, HO_2 and CH_2O) were obtained from at least one of, and in some cases, both the DC8 and P3B aircraft during the NASA Transport and Chemical Evolution over the Pacific (TRACE-P) campaign. To assess current understanding of fast photochemical processes that impact chemistry over the eastern Asia coast and western Pacific, these measurements are compared to theoretical predictions using a detailed photochemical time-dependent box model constrained by coincident measurements of critical long-lived tracers and physical parameters. HO_2 measured from the DC8 aircraft is consistently overpredicted by the model by a median of 23% with no apparent trend in the agreement with altitude. Three subsets of data composing 12% of the total number of HO_2 measurements represent outliers with respect to calculated-to-observed ratios of HO_2. Analysis of these subsets reveals various controlling factors that contribute to their deviation in agreement. In particular, data obtained within clouds show clear signals of HO_2 loss, presumably due to heterogeneous uptake. Alternately, observational evidence in support of heterogeneous loss to aerosol in cloud-free air is difficult to distinguish using this data set. OH is overpredicted in the upper troposphere by 80% for the DC8. In the middle troposphere, overpredictions are 60% for the DC8 and 40% for the P3B. Boundary layer and lower tropospheric OH calculated-to-observed ratios decrease from middle tropospheric values for both aircraft, to 1.07 for the DC8 and to 0.70 for the P3B. Highest concentrations of CH_2O near the coast are consistently underpredicted by the box model as a result of the inherent neglect of transport effects of both CH_2O and its precursors via the steady state assumption, though these occurrences are limited to only a few percent of the data (<1-5%). The steady state assumption for CH_2O is further tested using a global model environment in place of the real atmosphere. While results show this assumption is valid for most of the TRACE-P region, some evidence of transport effects shifting the CH_2O concentration away from steady state is captured by three-dimensional models. At lower background concentrations, box model predictions and observed CH_2O are in good agreement in the median, but a large scatter exists. Factors contributing to this scatter are examined, including the limited availability of some important constraining measurements. In particular, CH_2O was found to be quite sensitive to concentrations of CH_3OOH in regions of low NO_x, and for these regions, we identify observations of CH_3OOH as critical for obtaining more consistent assessments of CH_2O model-to-measurement agreement. Similar to previous analyses, methanol observations were shown to increase predicted CH_2O by 5-10% throughout the TRACE-P domain.

1 1. INTRODUCTION

2 NASA's Transport and Chemical Evolution over the Pacific (TRACE-P)
3 field campaign was conducted along the Asian Pacific Rim and the western Pacific
4 during February-April, 2001 [*Jacob et al*., 2003] with the aim to better understand how
5 outflow from the Asian continent affects the composition of the global atmosphere. *In-*
6 *situ* observational sampling of a broad suite of trace gases, aerosols, and
7 meteorological parameters were provided from two aircraft, NASA's DC8 and
8 P3B. The goals of TRACE-P were:
9 1) To determine the composition of Asian outflow over the western Pacific in
10 spring in order to understand and quantify the export of chemically and
11 radiatively important gases and aerosols and their precursors from the Asian
12 continent.
13 2) To determine the chemical evolution of the Asian outflow over the western
14 Pacific in spring and to understand the ensemble of processes that control this
15 evolution.
16 An examination of fast photochemical cycles and their role in processing the
17 chemical composition of Asian outflow is central to the second objective. Such
18 assessments of fast photochemistry must focus on short-lived chemical test species
19 that can be measured as well as theoretically predicted from *in situ* conditions.
20 In practice, and in order for theoretical predictions of fast photochemistry to maximize
21 the use of measured precursor species, the longer-lived precursor species are
22 constrained to measured values and a diurnal steady state modeling approach is used
23 to calculate fast photochemistry. Diurnal steady state is defined as reproducable

predicted concentrations over a 24-hour period. Because predictions of test species are based on a chemical diurnal steady state, their lifetimes must be sufficiently short to minimize effects due to air parcel aging. The accuracy of predictions are also subject to the quality of measurements of the longer lived species and other model inputs that regulate the concentrations of the short lived species.

Key test species available for examination in the TRACE-P data include nitrogen dioxide (NO_2), the hydroxyl (OH) and hydroperoxyl (HO_2) radicals, and formaldehyde (CH_2O). NO_X (NO_2 +NO) is the critical limiting precursor for O_3 production. HO_x ($OH+HO_2$) is central in the determination of the atmosphere's oxidative capacity and is pivotal to understanding photochemical ozone formation, removal of pollutant gases, and new particle formation. CH_2O plays an important role in the cycling of HO_x, particularly as it relates to the oxidation of non-methane hydrocarbons (NMHCs). While testing of NO_2 predictions has historically occurred during aircraft field campaigns [eg. see *Chameides et al*., 1990; *Davis et al*., 1993; *Crawford et al*., 1996], only recently have measurements of species such as HO_x allowed for a more detailed analysis of fast photochemical cycling. This paper presents results of an analysis of fast photochemistry using the measurements during the TRACE-P campaign.

2. MODEL DESCRIPTION

The analysis presented here is based on calculations from a time-dependent photochemical box model which has been described in detail in several previous studies (e.g., see Appendix of *Crawford et al*., [1999] for a detailed listing of reactions). Model-calculated species are assumed to be at diurnal steady state, meaning that

concentrations are integrated in time until their diurnal cycles no longer vary from day to day. The model chemistry includes basic HO_x-NO_x-CH_4 gas phase reactions based on the recommendations of *DeMore et al*. [1997] and *Atkinson et al*. [1992], with reaction and rate updates as in *Sander et al*. [2000]. The $O(^1D)$ quenching rate with nitrogen is updated as per *Ravishankara et al*. [2002]. Non-methane hydrocarbon (NMHC) chemistry is from the condensed mechanism of *Lurmann et al*. [1986] with modifications included to address remote low-NO_x conditions (e.g., formation of organic peroxides) and to represent explicit chemistry for acetone, propane, and benzene. Surface and heterogeneous losses for soluble species are simulated as in *Logan et al*. [1981].

Photolysis rate coefficients are computed using a DISORT four-stream implementation of the NCAR Tropospheric Ultraviolet Visible (TUV) radiative transfer code. These coefficients are initially based on a clear-sky assumption and are then adjusted to account for local radiative conditions. Model clear-sky photolysis rates are normalized throughout the day using a cloud correction factor (CCF) such that *in situ* spectroradiometer photolysis measurements are exactly matched at the time of the measurement [*Shetter and Müller*, 1999].

Model calculations use the 1-min merged data set available on the GTE TRACE-P public data archive (http://www-gte.larc.nasa.gov). Critical model input constraints include observations of O_3, CO, NO, temperature, dew/frost point, pressure, and photolysis rates, and model analysis is therefore limited to merged data points where this information is available. Non-methane hydrocarbons are constrained to observations where available (53% of the data), and are interpolated from adjacent

measurements in data gaps of less than 5 minutes (37% of the data). Data gaps of greater then 5 minutes were interpolated and examined subjectively for adequacy (10% of the data). Acetone, methyl ethyl ketone (MEK), methanol and ethanol are constrained to observations when data are available. In the upper troposphere, missing data for oxygenated hydrocarbons are filled using empirical relationships to CO derived from the TRACE-P data (see discussion in section 3). Additionally, because these model calculations show that methanol contributes a median of 10% to predicted CH_2O throughout the TRACE-P domain, missing data for methanol at altitudes below 8 km are filled based on its empirical relation to CO. Model analysis is limited to conditions with solar zenith angles less than 80°. The number 1-min merged points from the DC8 that meet the criteria for modeling is 5167 points, or 59% of the total, and 6621 points, or 70% of the 1-min merged points from the P3B, are analyzed.

In addition to the critical constraints described above, the model constrains the following species when measurements are available: Hydrogen peroxide (H_2O_2), methyl hydrogen peroxide (CH_3OOH), nitric acid (HNO_3), and peroxy acetyl nitrate (PAN). If unavailable, these species are calculated to be in diurnal photochemical equilibrium. With the exception of NO, constraining parameters are held constant throughout the diurnal cycle. Short-lived nitrogen ($NO+ NO_2+NO_3+2N_2O_5+HONO+HNO_4$) is photochemically partitioned at each time step while the total short lived nitrogen is held constant to a value such that predicted NO matches the measurement at the time of observation.

3. AVAILABILITY OF CRITICAL PRECURSORS FOR ANALYSIS OF HO_x and CH_2O

At upper tropospheric altitudes, oxygenated hydrocarbons such as acetone, MEK, methanol and ethanol can constitute an important primary source of HO_x [e.g., *Singh et al*., 1995; *Jaeglé et al*., 1998; 2000; *Crawford et al*; 1999]. The DC8, with a flight ceiling of 12 km, flies within this regime, and measurements of the above mentioned oxygenate species were obtained from this aircraft. Alternately, there were no measurements of oxygenates made on board the P3B during TRACE-P. The P3B flight ceiling is 7 km, however, which is below the altitude at which oxygenates are expected to become important components of the HO_x budget.

To confirm this expectation, Figure 1 shows the impact of oxygenates on HO_x using measurements from the DC8. This figure includes only those points with available oxygenate measurements. Results from two test simulations are shown relative to a base run that neglects oxygenates, illustrating the impact on HO_x from ketones (acetone and MEK; open boxes) and the combined impact from both ketones and alcohols (filled boxes). Increases in HO_x due to oxygenates are most significant in the upper troposphere (> 11 km), with enhancements of up to 60-80%. The figure shows a pronounced decline in the importance of oxygenates with lowering altitudes. Below 7 km, the median increase to HO_2 (OH) is predicted to be less than 5% (1%). Therefore, an analysis of fast photochemistry using data obtained from the P3B aircraft is not compromised by the absence of oxygenate data. Note that the majority of the increases shown in Figure 1 are attributed to acetone; MEK has only a limited role in the HO_x increases. Figure 1 also illustrates that the impact from alcohols is significantly less than the impact from ketones for HO_2 and is minimal for OH.

While measurements of acetone and other oxygenates were obtained on the DC8, data coverage for these species at the critical upper tropospheric altitudes of 8-12 km is only about 25%. Because of the significance of the oxygenate source contribution to HO_x at these altitudes, data points with missing upper tropospheric oxygenate data are filled based on empirical relationships derived from the TRACE-P data. The relationship between acetone in parts per trillion by volume (pptv) and CO in parts per billion by volume (ppbv) is found to be

Eq (1) Acetone (pptv)= -92.+6.27[CO (ppbv)].*

This relation gives an r^2 coefficient of 0.81 between observed and calculated acetone, with 75% of the errors less than 30% or 135 pptv. This derived relationship is similar to the empirical relation derived by *McKeen et al.* [1997] for data above 9 km in the western Pacific during February and March, 1994 during the PEM-West-B field campaign (*Acetone (pptv)=-126.8+6.12*[CO(ppbv)]*). MEK is assumed to equal a 5% fraction of the acetone mixing ratio. Methanol values are then scaled to acetone as:

Eq (2) Methanol (pptv) = .0284[Acetone (pptv)]$^{1.6.}$*

This equation gives an r^2 coefficient of 0.90, and 75% of the points have errors less than 16% or 245 pptv. Ethanol is assumed to equal a 5% fraction of methanol.

For the analysis of CH_2O, it is necessary to extend the data filling for methanol to altitudes below 8 km. The oxidation of methanol via OH can be a small but non-negligible source of CH_2O throughout the troposphere via:

(R1) $CH_3OH + OH (+ O_2) \rightarrow CH_2O + HO_2 + H_2O$

For example, *Frost et al*. [2002] showed that for 0-8 km during the NARE-97 campaign (North Atlantic Regional Experiment-97), an assumed methanol background of 700

pptv contributed just under 10% to the total CH_2O source. Methanol was measured from the DC8 during TRACE-P with a median value of 840 pptv. At these concentrations, the model calculations show that the median impact of CH_3OH oxidation on model-predicted CH_2O is on the order of 10%. Because the data coverage for CH_3OH on the DC8 below 8 km is 30%, missing methanol data points on that aircraft are filled based on simple empirical second-order polynomial fits to CO derived from the TRACE-P measurements. For altitudes < 2 km,

$$Methanol\ (pptv) = -400 + 5.7*[CO\ (ppbv)] + 8.9 \times 10^{-3}*[CO\ (ppbv)]^2,$$

with an r^2=0.84 and 75% of the errors less than 503 pptv or 75%. For altitudes from 2-8 km,

$$Methanol\ (pptv) = -469 + 13.2*[CO\ (ppbv)] - 1.1 \times 10^{-2}*[CO\ (ppbv)]^2$$

with r^2=0.6 and 75% of the errors less than 463 pptv or 50%. While the fits for methanol are noisier in the middle and lower troposphere than for the upper troposphere, the fits used here are a substantial improvement over filling methanol using simple median values.

A further source of uncertainty in model predictions of HO_x results from the limited availability of peroxide data. No peroxide data is available for the P3B aircraft, and measurements of H_2O_2 and CH_3OOH are available about half the time on the DC8. When measurements are unavailable, the peroxides are calculated under the assumption of photochemical equilibrium. However, deviations from equilibrium are expected due to wet removal and transport influences (e.g., convective transport of peroxides into the upper troposphere). Figure 2 shows the impact on calculated HO_x when peroxides are constrained to observations from the DC8 relative to results

obtained when the same set of points is run using model-calculated peroxides (i.e., unconstrained peroxides). While it may be argued that slight increases in HO_x (~10%) occur above 10 km as a result of peroxide constraints, the median ratio is near 1 throughout most of the troposphere. This indicates that while non-equilibrium conditions do exist for peroxides on a point-by-point basis, the overall bulk statistics for comparing measured and calculated HO_x should be relatively insensitive to peroxide constraints.

4. RESULTS

4.1 NO_x

The $NO+NO_2$ (NO_x) cyclic system is strongly coupled to the production of tropospheric ozone. The partitioning of NO_x varies significantly throughout the day and is dependent upon the abundance of sunlight and O_3:

(R2) $NO+O_3 \rightarrow NO_2+O_2$

(R3) $NO_2+hv \rightarrow NO+O$

(R4) $O+O_2+M \rightarrow O_3+M.$

Its partitioning is also influenced by the abundance of HO_2 and other peroxy radicals, which convert NO to NO_2, though the conversion due to reaction with O_3 *(R2)* is dominant (typically ~80% or more).

(R5) $HO_2+NO \rightarrow NO_2+OH$

(R6) $CH_3O_2+NO \rightarrow NO_2+CH_3O$

(R7) $RO_2+NO \rightarrow NO_2+RO.$

Equilibrium partitioning normally occurs on timescales of minutes and can thus be estimated using the simple assumption of photostationary state.

NO_2 has long been used as a test species for fast photochemistry in field campaigns because of its long history of measurements and its involvement in the cycling of HO_x (e.g., see *Chameides et al*. [1990], *Davis et al*. [1993] and *Crawford et al*. [1996]). Note, however, that although NO_2 can be influenced by HO_2, it is difficult to determine HO_x directly from NO and NO_2 photostationary state because of the dominance of O_3 in converting NO to NO_2 *(R2)*.

Onboard the DC8, NO and NO_2 were measured using photofragmentation two-photon laser-induced fluorescence (TP-LIF) [*Sandholm et al*., 1997, and references therein]. Precision and accuracy of this instrument are reported as 40%, and data coverage for NO_2 is approximately 70% for the modeled subset of data points. Measurements of NO_x on the P3B were obtained using a photolytic conversion technique followed by chemiluminescence detection of NO [*Nakamura et al*., 2003]. The accuracy and precision are reported as 32% and 4 pptv for a 10 s integration time, and data coverage for NO_2 is 65% of the modeled points.

Figure 3 shows calculated-to-observed ratios (calc/obs) for NO_2 from both the DC8 and P3B aircraft as a function of altitude. The median calc/obs ratio for the DC8 is near 1, with an r^2 correlation coefficient of 0.80 for the full data set. When considering NO_2 data less than 100 pptv (nearly 90% of the data set), the median calc/obs ratio remains equal to 1 while r^2 decreases to 0.62. This is similar to that found during the GTE PEM-Tropics campaigns [*Olson et al*., 2001].

On the P3B, the median NO_2 calc/obs ratio shows a bias of 1.25, with a correlation coefficient equal to 0.88 for the full data set. This high correlation, like for the DC8, is also driven by the extreme data points; for NO_2 less than 100 pptv

(representing 80% of the P3B data), the median ratio decreases only slightly to 1.20, and the scatter is very similar to that for the DC8 (r^2 = 0.6). *Nakamura et al*. [2003] find that the calc/obs bias does not improve for points where peroxy radicals are negligible, i.e., where the NO/ NO_2 cycling is dominated by well established reactions involving the measured quantities O_3, NO and the photolysis rate for NO_2. Thus it is unlikely that the systematic bias in NO_2 could be ascribed to any deficiency in current understanding of HO_x photochemistry. Figure 3 also shows that the calc/obs bias for P3B NO_2 shows an altitudinal dependence, with ratios less than or close to 1 at altitudes above 4 km. Our analysis suggests this trend appears to be most closely tied with altitude, rather than absolute concentration. This is consistent with the conclusions of *Nakamura et al*. [2003], who also show that interferences from NO_y species in these colder temperatures are unlikely to contribute at a magnitude large enough to influence this bias, so the cause of the altitude trend in the calc/obs ratio remains uncertain. The potential interference resulting from decomposition of NO_y species on the wall of the photolysis cell, however, has not yet been determined due to technical difficulties.

While about half of the points on the P3B and 42% of the points on the DC8 show NO_2 calc/obs ratios outside the range of instrument accuracies, differences between NO_2 predictions and measurements are not large enough to significantly influence predictions of HO_x.

4.2 HO_x

Tropospheric HO_x is central to tropospheric chemistry and the oxidative capacity of the atmosphere. OH is the major oxidizing agent for a host of chemical species

including greenhouse gases, and the HO_2 radical is a key component in the production of tropospheric O_3. In the lower troposphere, the principal source of HO_x is from the reaction of the excited state $O(^1D)$ with water vapor following O_3 photolysis. In the presence of extremely low water vapor (e.g. upper troposphere), photolysis of acetone can become the dominant source [*Singh et al*., 1995]. Secondary production of HO_x stems from the oxidation of non-methane hydrocarbons (NMHC). Though this process initially consumes OH, further reactions of products from NMHC oxidation such as formaldehyde (CH_2O) can in turn produce multiple HO_2 radicals. Additionally, species such as peroxides that are typically considered to be in equilibrium with HO_x can become local sources when transport-induced non-equilibrium conditions occur, such as the convective transport of abundant peroxides from the boundary layer into the free troposphere [*Jaeglé et al*., 1997; *Prather and Jacob*, 1997]. Major HO_x losses include the self reaction of HO_2 to form H_2O_2, reaction of OH with HO_2, and reaction of OH with NO_2 to form HNO_3. Internal recycling of HO_x is largely dependent on NO and CO, and is important in defining both the O_3-forming potential of the environment, and in the efficiency of the HO_x sinks.

Only since the 1990s, have direct measurements of HO_x been implemented from airborne platforms. Early measurements of OH in the lower troposphere from the ACE-1 [*Mauldin et al*., 1998] and PEM Tropics A [*Mauldin et al*., 1999] field campaigns showed modeled OH values were typically slightly higher than measurements. The first upper tropospheric measurements, from the STRAT and SUCCESS campaigns indicated that the HO_x abundance at higher altitudes exceeded expectations based on current theory by factors of up to 2-4 [*Jaeglé et al.*, 1997; *Wennberg et al*., 1998; *Brune*

et al., 1998]. In addition to a severe model underprediction of HO_2 during the SUCCESS field campaign, a bias in the HO_2/OH ratio was found, with the observed ratio being an average of 30% higher than that predicted by models [*Brune et al*., 1998]. It was theorized that convective transport of HO_x precursors such as peroxides and formaldehyde might explain the HO_x imbalance in the upper troposphere [*Jaeglé et al*., 1997; 1998*; Prather and Jacob*, 1997], but the lack of measurements for these precursors prevented a definitive investigation.

Later field campaigns provided time-coincident measurements of both HO_x and precursors. During SONEX, general agreement with models was good, but it was found that peroxide transport played only a minor role in determining HO_x abundance during that campaign [*Jaeglé et al*., 2000]. PEM-Tropics B provided the first measurements of HO_x and its precursors concentrated in the tropical environment. While the median overall agreement was good, for the first time the upper tropospheric model calculations of HO_2 were greater than reported measured values. Conversely, OH calculations were lower than reported measured values in the upper troposphere, leading to a 30% model overestimation of HO_2/OH, a bias equal to that during SUCCESS [*Olson et al*., 2001].

4.2.1. HO_x model-to-observations comparisons during TRACE-P

During TRACE-P, measurements of HO_x were obtained from both aircraft. Onboard the DC8, OH and HO_2 measurements were obtained with the Penn State Airborne Tropospheric Hydrogen Oxides Sensor (ATHOS), which employs a laser induced fluorescence technique, the same instrument used during the SUCCESS, SONEX, and PEM-Tropics-B field campaigns [*Brune et al*., 1995]. Measurements of

OH and HO_2 are reported at a frequency of every 10 seconds with an estimated absolute accuracy of 40% and a limit of detection of 0.1 pptv for HO_2 and 0.01 pptv for OH. Data for HO_x are reported for 93% of the modeled data points (over 4800 points).

On the P3B, OH measurements were made using a multi-channel selected ion chemical ionization mass spectrometer system with a reported error of 60% [*Mauldin et al.*, 2003] and a data coverage of 75% of the modeled points. While HO_2 measurements were also obtained, using a chemical ionization mass spectrometer [*Cantrell et al.,* 2003], coverage with this technique was sparse and are not included in this analysis of HO_x measurements during TRACE-P.

Though the model persistently overpredicts DC8 HO_x throughout the troposphere during TRACE-P, 75% of HO_2 points and 48% of OH points are within the stated measurement accuracies. Eighty-five percent of the P3B OH points are within the stated measurement accuracy of +/- 60%. The model-to-measurement comparisons are shown in Figure 4 for OH and in Figure 5 for HO_2. The median OH calc/obs ratio on the DC8 is 1.4 with a clear altitude dependence; the ratio increases from a 7% overprediction for altitudes below 1 km to a 60% overprediction in the middle troposphere and an 80% overprediction at the highest altitudes (Figure 4a, open boxes). This general altitude trend is duplicated in the P3B data, though the profile is shifted toward lower ratios; boundary layer P3B model generated OH is underpredicted by 30% relative to measurements, and is overpredicted by 40% at altitudes near 6 km.

HO_2 on the DC8 shows a median model overprediction of 1.23 with no evident altitude dependence (Figure 5a). Note that the outlier points for HO_2 which fall below the agreement line at low mixing ratios on Figures 5b are largely associated with

stratospheric air and will be discussed in a later section. Similar outlier points at low mixing ratios for the DC8 OH (Figure 4b) are associated with high solar zenith angles.

While both OH and HO_2 measured on the DC8 have a reported accuracy of +/- 40%, the broader range of ratios for OH reflects the lower measurement precision for this species which is derived from a much smaller signal than for HO_2 [*Faloona et al*., 2000]. From the lack of an altitude dependence in HO_2 calc/obs, it follows that the HO_2/OH calc/obs ratio is inversely related to the altitude dependence of OH, with a 20% overprediction near the surface, decreasing to an underprediction above 8 km of 23%, a value similar to the upper tropospheric underpredictions of this ratio during both PEM-Tropics-B and SUCCESS.

4.2.2. Discussion of HO_x comparison.

While there is a consistent bias in the DC8 HO_2 model-to-measurement comparison of 23% during TRACE-P, the point-to-point correspondence is quite compact (r^2=0.88, Figures 5a and 5b). Most of the data is well-behaved, which allows for identification of subsets that are clearly outliers from the preponderance of the data. Three subsets, constituting a total of 12% of the modeled HO_2 points, are identified in Figure 6a, which shows the individual DC8 HO_2 calc/obs ratios as a function of altitude. These subsets, with a behavior distinct from the majority of the data, are defined as in-cloud data (6.4%), high O_3 or stratospheric (2.3%), and high altitude/high NO (3.3%).

Table 1 shows median statistics for the two outlier subsets that are predominantly in the upper troposphere (> 7 km); stratospheric data and high NO data. Statistics for the remaining data points at those upper altitudes are also shown, identified here as ‘majority data’. The first subset includes points of likely stratospheric

origin, subjectively identified using O_3 greater than 120 ppbv. These data are shown with purple diamonds in Figure 6. Table 1 confirms that these points are associated with very high O_3, low water vapor, CO and hydrocarbons, and moderate NO_x, consistent with stratospheric influence. The median HO_2 calc/obs ratio for the stratospheric points is 0.63, significantly less than the 1.24 median calc/obs ratio for the majority data. In addition, the median OH calc/obs ratio for the stratospherically influenced points is 0.77, in stark contrast to a median value of 1.64 for the majority.

A second outlier subset consists of upper tropospheric NO values greater than 135 pptv, shown with red triangles in Figure 6. These points are likely associated with convected pollutants, since CO, O_3, and hydrocarbons are slightly elevated above that for the majority subset. The HO_2 calc/obs ratio is 0.97, lower than the majority subset ratio. This decrease in ratio with increasing NO concentration is consistent with the general behavior found by *Faloona et al.* [2000] in examination of SONEX and SUCCESS data. In contrast to the stratospheric points, however, the OH calc/obs ratio is quite large, with a value of 2.01. Such behavior is suggestive of an uncertainty related to the rate of HO_x recycling by NO.

Note that data with NO greater than 135 pptv also occurs in the lower troposphere, indicated in Figure 6 by gray triangles. However, only those high NO points at altitudes greater than about 6 or 7 km show a HO_2 calc/obs behavior distinct from the preponderance of the data. Below 6 km, the median HO_2 calc/obs ratio for the high NO data (gray triangles) is 1.23, identical to the bulk median. Therefore, the HO_2 calc/obs discrepancy associated with high NO appears to be limited to the upper troposphere.

Selected HO_x source and loss terms for the data subsets in Table 2 reveal clear differences between the subsets in the dominant instantaneous processes affecting HO_x. While acetone concentrations are quite low for the stratospheric points and the water vapor reaction with $O(^1D)$ is the major HO_x source for this subset of points, acetone photolysis increases somewhat in its importance for the high NO data and majority data, where acetone concentrations are much larger than for the stratospheric subset.

It is exceedingly difficult to significantly impact calculated HO_x by adjustments in the primary source or losses because HO_x is a highly buffered system [Wennberg *et al*., 1998; *Crawford et al*., 1999]. This is evident in examining the sensitivity of model calculations to the uncertainty in water vapor measurements for the stratospheric subset of data. Note that to bring the calc/obs ratios for the stratospheric HO_2 into agreement with measurements, HO_2 would need to increase by nearly 40%, and to come into agreement with the majority data subset (where calc/obs = 1.24) an HO_2 increase of 107% is required. During TRACE-P, measurements of water vapor were obtained from a diode laser instrument which recorded significantly larger concentrations of H_2O than the cryogenic hygrometer under dry conditions; for the stratospheric points, median H_2O measured by the diode laser was 2.4 times larger. When the diode laser H_2O was used in model calculations, predicted HO_2 increased by about 17% which falls far short of explaining the discrepancies in the HO_2 calc/obs ratios shown in Table 1. Similarly, an increase of acetone by 25%, the stated measurement uncertainty, increases HO_x for the High NO subset, where acetone is a relatively significant primary source, but only by about 5%.

Selected HO_x loss rates are also shown in Table 2. Losses due to HO_x self reactions for the majority data subset are clearly dominant over the reservoir HNO_3 formation ($OH+NO_2$) by a factor of 50. In the lower HO_x environments of the high NO and stratospheric subsets, on the other hand, the HNO_3 formation reaction contributes to the HO_x loss at a much greater relative rate, with the loss for the stratospheric subset nearly equal to the HO_x self reactions. Thus uncertainties in the HO_x self reactions can be expected to have a greater influence on the majority data subset HO_2 than for the stratospheric or high NO data subsets. The uncertainty in the $OH+HO_2$ rate at 225 K is on the order of 50% [*Sander et al.*, 2000], while that for HO_2+HO_2 is slightly larger, on the order 75% for upper tropospheric conditions [*DeMore et al.*, 1997]. If these rates were held to the higher ends of their respective uncertainties, increasing the HO_x loss, calculated HO_2 decreases for all data, but only somewhat more significantly for the majority data. The spread between median calc/obs ratio between the subsets does not change significantly; median HO_2 calc/obs ratio decreases to 0.58 and 0.85 for the stratospheric and high NO subsets and to 1.05 for the majority data. This uncertainty is clearly not adequate to explain the differing behaviors between the subsets.

Uncertainties in the formation of HNO_4 (HO_2+NO_2) [*Sander et al.*, 2000], which can be a component in the HO_x budget (Table 2), are not large enough to alter predictions of upper tropospheric HO_x by more than about 15%. Similarly, uncertainties in the $OH+NO_2$ rate are not large enough to significantly impact predictions of HO_x. Further, the uncertainty in the equilibrium constant for HNO_4 has minimal impact on the HO_2 deviation [*Faloona et al.*, 2000]. Thus though these subsets reveal different dominating processes in the HO_x budget, along with different behaviors of the HO_2

calc/obs ratio, uncertainties in primary source components or HO_x loss processes are not sufficient to explain the differences.

Discrepancies between the stratospheric subset and the majority data subset extend beyond HO_x to CH_2O. As discussed earlier, CH_2O photolysis can be an important secondary source of HO_x in the upper troposphere; CH_2O is a photochemical byproduct of acetone and hydrocarbon degradation. For the stratospheric subset, the median measurement reported for CH_2O is 55 pptv. An important caveat to note, however, is that most of these reported values are under the instrument LOD (*Fried et al.*, [2003a], and see CH_2O LOD discussion in section 4.3). Nevertheless, this implies measured CH_2O may be up to three times larger than that calculated by the model, which has a median value for the stratospheric subset of 17 pptv. If the stratospheric points are modeled whilst constraining CH_2O to the median measured value of 55 pptv, median predictions of OH and HO_2 increase by 71% and 79% respectively, increasing the median OH calc/obs ratio to 1.28 and the HO_2 calc/obs ratio to 0.95. Note, however, that CH_2O levels of 55 pptv cannot be supported by the concentrations of acetone or other hydrocarbons measured.

The data points marked with a green asterisk in Figure 6 indicate a third subset: within-cloud data as determined by a combination of visual inspection of flight videos and measurements of particles in the 10-20 micron range from the Forward Scattering Spectrometer Probe (FSSP). Median HO_2 calc/obs ratio for data points which were determined to be within clear air was 1.23, while that for in-cloud data points increased by 25% to 1.55. In general, the large model overpredictions for HO_2 in clouds are

consistent with a heterogeneous HO_x loss within clouds which is not included in the base model calculations.

A heterogeneous loss of HO_2 to clouds and aerosol was added for a test model simulation, with a heterogeneous loss rate (k_{het}) parameterized as

$$\textit{Eq (5)}\quad k_{het} = \int_{a_{\min}}^{a_{\max}} \frac{n(a)4\pi a^2}{\left(\frac{a}{D_g} + \frac{4}{\upsilon\gamma}\right)} da,$$

where *a* is the effective particle radius for a given observational size bin, *n(a)* is particle number size distribution, D_g is the gas-phase molecular diffusion coefficient of HO_2, υ is the mean molecular speed, and γ is a reaction probability which is set to 0.2, as is suggested in *Jacob* [2000]. The integral is evaluated over the all available particle size spectrum observations by the FSSP and OPC (Optical Particle Counter) instruments onboard the DC-8 aircraft. The size range of these observations falls primarily within 0.1 to 50 μm. The median decrease in calculated HO_2 due to in-cloud heterogeneous loss is 70%, bringing the median in-cloud calc/obs HO_2 ratio to 0.42 (Figure 6b, green asterisks). While the loss calculated using *Eq (5)* is therefore clearly not consistent with observations, the error in estimated cloud aerosol number/size distribution is on the order of 100% so the heterogeneous loss parameterization is highly uncertain and there may be other HO_2 loss limiting factors which are not described in *Eq (5).* Furthermore, heterogeneous losses to HO_x precursors and/or reservoir species were not considered in this assessment (e.g., CH_2O and H_2O_2; see *Fried et al*. [2003a]). Nevertheless, Figure 6 suggests observational evidence supportive of the impact of heterogeneous removal of HO_2 within cloudy regions.

With the described outlier subsets removed (stratospheric, high altitude/high NO, and in-cloud), the remainder of the data points is compact (Figure 6a, black points), with little altitudinal variation; the r^2 improves from 0.88 to 0.91 and the standard deviation improves from 0.55 to 0.49. The median impact on HO_2 from heterogeneous loss to aerosol in clear air (no cloud) can also be seen in Figure 6b, and is calculated to be on the order of a 3% decrease, with maximum decreases in the boundary layer (7%) and minimum decreases in the upper troposphere (1-2%). Therefore because the heterogeneous aerosol effect is expected to be so small, the HO_2 measurement is not sensitive enough to independently verify the magnitude of this HO_2 loss.

4.3 Formaldehyde

Formaldehyde is an intermediate product in the oxidation by OH of methane and other hydrocarbons; its major global source is photochemical production. In addition, CH_2O is directly emitted from industrial combustion and biomass burning, though these sources are expected to be relatively minor [*Sigsby et al.*, 1987*; Lee et al.*, 1997]. CH_2O losses include oxidation by OH and photolysis. Photolysis proceeds through two branches, one of which leads to formation of HO_x, while a secondary branch leads to stable products. Thus the photochemical cycling of CH_2O is intimately tied to both hydrocarbon degradation and HO_x formation. This, along with the fact that CH_2O can be more sensitive than HO_x to changes in precursor species makes it a particularly important test species for improving our understanding of photochemical cycling [*Crawford et al.* 1999].

Measurement-to-model comparisons of CH_2O have a long history, particularly in the remote troposphere. Such comparisons have exhibited both positive and negative deviations, as well as good agreement. In the marine boundary layer, models have overpredicted CH_2O relative to measurements [*Lowe and Schmidt*, 1983; *Jacob et al.* 1996*; Liu et al.,* 1992; *Zhou et al*., 1996] as well as underpredicted CH_2O [*Weller et al*., 2000; *Ayers et al*., 1997]. Models have typically underpredicted CH_2O in the middle and upper troposphere [*Jaegle et al*., 2000; *Heikes et al*., 2001; *Fried et al*., 2002; *Frost et al.,* 2002]. Two recent studies have shown good agreement on average between CH_2O model predictions and measurements: *Fried et al.* [2003b] during the TOPSE 2000 airborne campaign, and the shipboard studies by *Wagner et al.* [2002]. *Wagner et al.* [2002] also presented results from a conservative uncertainty analysis of both theory and measurements which concluded that deviations between models and measurements as large as 65% are not significant.

During TRACE-P, two independent instruments measured formaldehyde on board the DC8: a coil enzyme method [*Heikes et al*., 1996] and a tunable diode laser absorption spectrometer [*Fried et al*., 2003a]. For this analysis, we focus on model comparisons with data from the laser spectrometer, which has 80% data coverage within the 1-min merge. Note that a CH_2O model-measurement comparison using these data and model results are also extensively discussed in *Fried et al*. [2003a]. Values of the 2σ LOD (limit of detection) for the laser spectrometer were typically between 60 and 80 pptv [*Fried et al*., 2003a], and one-third of all measured CH_2O was at LOD. This percentage is greatest at upper altitudes, with 60% of the measurements above 8 km below LOD. As discussed by *Fried et al*. [2003a], CH_2O concentrations are reported for

all data, including those at and below LOD. To avoid biasing our comparison, we retain those measurements below LOD for our analysis.

A scatter plot of modeled versus observed formaldehyde is shown in Figure 7a, with a smoothed version of the data used in Figure 7b. Note that some of the data below LOD were reported as negative and do not appear on these logarithmic plots. To create the smoothed data, measurement-model data pairs were first sorted by model concentration, and measurements were then smoothed using a 1% running average. This analysis is equivalent to a binning approach (e.g., see *Fried et al*. [2003a]). By sorting the data pairs using model concentration rather than measurement, the smoothing process eliminates negative values and allows for an assessment of the reported LOD.

For the full raw dataset (Figure 7a), the median calc/obs ratio for CH_2O is 0.92, with an r^2 correlation coefficient of 0.85. However, the general behavior of the model-to-measurement comparison differs distinctly across the spectrum of measured CH_2O mixing ratios. This behavior within the data is more clearly evident when smoothing the data (Figure 7b). In this figure, calculated CH_2O agrees well with observed values for mixing ratios of roughly 60-500 pptv. Here, the slope of the agreement equals 1.02, indicating no bias in the model-to-measurement comparison. These results corroborate those shown in *Fried et al*. [2003a], who employ a binned regression analysis approach. Below about 60 pptv, the measurement-model correlation degrades for this comparison, which agrees with the reported 1-minute LOD of *Fried et al.* [2003a]. Note, however, that as discussed in *Fried et al*. [2003a], longer measurement averages can in some instances be employed during stable horizontal flight legs to improve the

measurement precision. For concentrations greater than 500 pptv, the slope differs markedly, with a value of 0.37, as the model increasingly underpredicts CH_2O at the highest concentrations.

4.3.1. The impact of transport on CH_2O predictions

One possible explanation for the underprediction of CH_2O at highest concentrations is that direct transport of CH_2O and its precursors plays an important role in these data. In regions within near-coast pollution plumes, the impact of direct sources and short-lived precursors such as ethene could shift the concentration of CH_2O away from photochemical steady state. Because the median lifetime of CH_2O for the daylight TRACE-P calculations is 2.2 hours, locations where direct physical transport becomes significant enough to nudge its concentration away from steady state are limited to within a few hours of large emission areas. Note that the transport distance would increase for nighttime emissions, when the instantaneous CH_2O lifetime is longer. Evidence of fresh continental pollution only a few hours removed from the coast was encountered on more than one occasion during TRACE-P, particularly during DC8 flights over the Yellow Sea (e.g., Flights 9 and 13).

Figure 8 illustrates that the geographical location of significant model underpredictions of CH_2O in high concentration areas are indeed limited to the Yellow Sea region. Figures 8a and 8b show the location of all CH_2O measurements by the laser spectrometer, and of all measurements greater than 500 pptv, respectively. Measurements greater than 500 pptv constitute 7% of the total CH_2O measurements. While there are many isolated measurements exceeding 500 pptv, it is difficult to arbitrate the model versus measurement disagreement given the scatter shown in

Figure 7a. Instead, extended periods of high CH_2O concentration are isolated based on averaging over horizontal flight legs to remove much of the noise. Figure 8c identifies points within these horizontal flight legs where the average CH_2O measurement exceeds 500 pptv. These occurrences reduce the number of identified points to 3% of the data set, and are limited to the Yellow Sea plus a few locations further offshore. Figure 8d shows only those flight legs for which the calc/obs ratio is less than 0.7, which constitute about 1% of the total observations. Note that for the remainder of the points with flight leg averages larger than 500 pptv, the average calc/obs ratio is 0.96, indicating no substantial bias in the model prediction. The fact that the large underpredictions are exclusively located in the Yellow Sea and at low altitudes (below 2.5 km) is highly suggestive of transport effects. This qualitative exercise suggests that during the overall TRACE-P campaign, transport influences affecting CH_2O were quite rare, impacting on the order of only a few percent of the data.

To further explore possible errors introduced by the steady state assumption for CH_2O, particularly due to pollutant transport, a sensitivity test was undertaken, using results from version 4.33 of the Harvard 2 x 2.5 GEOS-CHEM global model simulation for the TRACE-P time period in place of observational data (http://www-as.harvard.edu/chemistry/trop/geos/geos_version.html; *Evans et al., manuscript in preparation*). The box model analysis was repeated using GEOS-CHEM global model parameters from along simulated flight tracks through the model environment as box model constraints. The box model photochemical steady state predictions for formaldehyde were then compared to those predicted by GEOS-CHEM, which includes simulated effects of both photochemistry and transport. Note that to effectively use this

exercise as a method of extracting any modeled non-equilibrium behavior of CH_2O by GEOS-CHEM, various minor adjustments to the box model chemical mechanism were required in order to more closely mimic the photochemical mechanism used in the Harvard model.

Results from this exercise are shown in Figure 9 as box model/GEOS-CHEM CH_2O ratios. The median ratio is 0.92. This small bias is most likely a result of remaining minor input and mechanistic differences between the two models. The agreement is compact, with an r^2 correlation coefficient of 0.93, suggesting that the assumption of steady-state for formaldehyde is appropriate throughout most of the TRACE-P region. The data in Figure 9 show some areas where the ratio is significantly different than one. The few high altitude outliers are points where CH_2O is at concentrations less than 35 pptv and the median box model overprediction is on the order of 10-15 pptv, resulting in inflated ratios. Most of the scatter, however, is located in the lowest few km, where ratios both greater than and less than 1 are seen. Outlier ratios greater than 1 are associated with GEOS-CHEM CH_2O less than then median (500 pptv), while outlier ratios less than 1 are associated with the higher CH_2O concentrations in GEOS-CHEM.

Figure 10a shows the box model/GEOS-CHEM CH_2O ratios for the upper 50^{th} percentile of the observed concentrations. There is a slightly greater tendency for box model underpredictions at the highest end of concentrations, though not as pronounced as for the observational TRACE-P analysis (shown in Figure 10b). Both sets of data have an overall median ratio near 0.9, and median ratios for segments of tenths of percentiles are indicated on the figures. The uppermost 10^{th} percentile segment ratio

for GEOS-CHEM decreases abruptly from 0.91 to 0.85 and that for the observed data gradually but steeply decreases to 0.69 for the upper 10^{th} percentile.

Figure 11 shows the geographical location of the significant box model underpredictions of GEOS-CHEM CH_2O > 500 pptv. As for Figure 8d, points where box model/GEOS-CHEM ratios are less than 0.7 at concentrations of greater than 500 pptv are shown. These points constitute 1.1% of the Harvard data set, which is similar to the small fraction affected by transport in the observational data set. About 15% of these identified points reside in the Yellow Sea and slightly more than half of the points lie approximately 1000 km south or southwest of Japan, or on the order of a day's transport time from the coast, with the rest located off the coast of Taiwan. Therefore, while the box model analysis using both the observational data and the GEOS-CHEM analysis suggest there are isolated cases where transport may influence CH_2O, the portion of the data affected is very small, on the order of a few percent or less.

4.3.2. Impact of constraining species on the model-measurement comparison.

Model-measurement agreement is quite good for data falling between the measurement LOD and 500 pptv, but this agreement is not readily apparent without smoothing the data. The comparison in Figure 7a is quite scattered for data below 500 pptv (r^2 = 0.46), and this noise is likely to be due to a variety of causes. Some of these include uncertainties in the measurement (2σ LOD ~ 60-80 pptv) or in the model mechanism, uncertainties in the modeling approach (e.g., treatment of clouds), and uncertainties in formaldehyde precursors, which encompass both the limited availability of precursor constraints and also measurement issues (e.g., unmeasured hydrocarbon

species or uncertainties in measurements of precursors such as CH_3OOH). *Fried et al*. [2003a] also discuss some aspects of measurement and model uncertainties.

As noted earlier, this modeling study is limited by the availability of several important but noncritical model inputs. These input species, which include peroxides H_2O_2 and CH_3OOH), PAN, and HNO_3, are constrained to observations at points where data are available and are calculated where observations are missing. The uncertainty imposed by the limited availability of these constraining species becomes most obvious in calculations for periods of flight through homogeneous air masses. If model predictions of these species are significantly different than adjacent measurements, the result is an oscillation between the measured value (when available) and the calculated value. Depending on the sensitivity of CH_2O to variations in these constraining species, this in turn can potentially introduce oscillations in the time series of calculated CH_2O (also see discussion in *Fried et al*. [2003a]). Further complicating things, some periods of oscillatory behavior are seen in the TRACE-P data where the presence of a constraining measurement improves model-measurement agreement while other periods clearly exhibit better agreement when constraining species are absent.

To evaluate the sensitivity of CH_2O to the availability of noncritical constraint species, we ran several independent model tests. For each mixed constraint species tested (e.g., CH_3OOH), that set of points with valid measurements was rerun with the test species unconstrained (calculated), rather than constraining it to observations. Differences in predictions of CH_2O were then examined as a function of the differences in unconstrained and constrained values of the test species.

Tests for HNO_3 showed that CH_2O was insensitive to its variations, precluding the need for further discussion. Results from test simulations for CH_3OOH, H_2O_2 and PAN are shown in Figure 12. The top row of plots (Figures 12 a, b, and c) shows relative differences for the unconstrained (calculated) values versus constrained (observed) values for the relevant species; thus, values greater than one indicate a model overprediction. The y-axis shows relative differences in predicted CH_2O for the unconstrained versus constrained runs. The bottom row of plots in Figure 12 (d, e, and f) shows absolute differences for the test species and for CH_2O (unconstrained minus constrained). The distribution and range of the variations in the test species is a measure of the ability of the steady state model to predict their concentrations, and the corresponding response in predicted CH_2O may be interpreted as one measure of the variance potentially introduced as a result of the limited availability of these constraining species.

It is apparent from Figure 12 that for background concentrations of CH_2O, variations in CH_3OOH are the most critical of the constraints. Absolute differences in CH_2O of up to several hundred pptv are computed, with relative ratios ranging from as low as 0.3 to as high as 3.50. The colors in Figure 12 indicate the level of NO; blue points show data where NO was less than 5 pptv, and red points show data where NO was measured at greater than 50 pptv. Figure 12a indicates that CH_2O is particularly sensitive to CH_3OOH when NO levels are very low, also discussed in *Fried et al*. [2003a]. Under these conditions, formaldehyde production becomes dominated by photolysis of CH_3OOH (*R11*, shown below) as the production from the methyl peroxy radical reaction with NO becomes small (i.e., *R8*).

(R8) $CH_3O_2 + NO\ (+O_2) \rightarrow CH_2O + 2\ HO_2 + NO_2$

(R9) $CH_3O_2 + HO_2 \rightarrow CH_3OOH + O_2$

(R10) $CH_3O_2 + CH_3O_2 \rightarrow 2CH_3O+O_2$

$\rightarrow CH_2O + CH_3OH$

(R11) $CH_3OOH + hv\ (+O_2) \rightarrow CH_2O + HO_2 + OH$

(R12) $CH_3OOH+OH \rightarrow CH_3O_2+H_2O$

$\rightarrow CH_2O + OH+ H_2O$

Additionally, note that CH_3OOH is frequently overpredicted by the model under low NO conditions (i.e., 80% of the blue points in Figure 12a are greater than one.). One possible explanation for this is a box model overestimation of the peroxy radical production of CH_3OOH *(R2)* by the steady state approach which neglects any time evolution of intermediate-lived species such as NO_x, particularly in the presence of upstream emissions. Such an effect is also suggested by *Wang et al*. [2002] in a similar type of steady state box model analysis using data over the northern and middle high latitudes from the TOPSE field campaign. Additionally, *Fried et al*. [2003a] propose the possibility that reactions of CH_3OOH on aerosols and/or with halogens may be important and result in model underpredictions of this species under low NO conditions.

The impact of H_2O_2 and PAN constraints on CH_2O are lower. Although there are some cases of CH_2O absolute differences on the order of a hundred pptv for underpredictions of PAN (Figure 12f) the relative impact on CH_2O remains low (Figure 12c). This is because underpredictions of PAN are limited to polluted conditions where CH_2O mixing ratios are already elevated.

While these exercises illustrate the sensitivity of CH_2O predictions to CH_3OOH, it is useful to determine how often this oscillatory behavior occurs in the field data and whether it impacts the gross statistics of the comparison. Within the lowest 2 km, we identified 175 CH_2O data points that were located within 7 constant-altitude legs where differences in constrained and unconstrained CH_3OOH were at least 250 pptv, and where resulting model predictions of CH_2O oscillated by at least 30% as a result of the CH_3OOH differences. These 175 flagged points constitute about 13% of all CH_2O data at those altitudes. Above 2 km, such oscillations do occur, but are rarer; we identified 75 CH_2O data points within 4 legs that displayed such oscillatory behavior, which is only about 2% of the data.

Because the oscillatory behavior occurs most frequently in the lowest 2 km, we examine the model to measurement comparison of CH_2O at these lower altitudes. For all lower altitude CH_2O below 500 pptv, the median calc/obs ratio is 1.03, with a model versus measurement r^2 correlation of 0.2. If we segregate the data into subsets that include constrained CH_3OOH and unconstrained CH_3OOH the median CH_2O ratios are somewhat different between the subsets, with the constrained CH_3OOH data resulting in a decreased median calc/obs CH_2O of .91 and the unconstrained data giving a larger ratio of 1.12. While this result establishes that limited observations of CH_3OOH is a source of uncertainty in model-measurement comparisons, it is interesting to further note that the correlation r^2 between calculated and observed CH_2O is unchanged when limiting the comparison to either the constrained or the unconstrained subsets of calculations. Thus, other sources of uncertainty must play a role. These of course include uncertainty in both the CH_2O measurements themselves as well as the

uncertainty in constraining measurements. What is clear from this exercise is the sensitivity of CH_2O predictions to presumed concentrations of CH_3OOH. Therefore, in order to more accurately assess formaldehyde measurements, accurate measurements of CH_3OOH, particularly in low NO_x regimes, are critical.

4.3.2. Impact of clouds on predictions of CH_2O.

Fried et al. [2003a] discuss the role of local within-cloud heterogeneous loss of CH_2O that is not specifically reproduced by the box model which assumes a climatological wet loss throughout the troposphere but does not simulate instantaneous in-cloud removal. *Fried et al*. [2003a] conclude that model predictions of CH_2O can be up to 56% larger than observed within cloudy regions as a result of this effect.

Another impact related to clouds that affects predictions of CH_2O is the application of the cloud correction factor (CCF; see Section 2). For example, at very low or very high CCF (i.e. when in an environment with heavy cloud attenuation or high reflectance), the assumption that these extreme cloud influences persist throughout the diurnal cycle is most likely erroneous. Approximately 10% of CH_2O data below 500 pptv fall under these extreme conditions, identified as CCF(JO^1D) less than 0.5 or greater than 1.7. For CCF(JO^1D) values less than .5, the median CH_2O ratio is 0.67, and for CCF(JO^1D) greater than 1.7, the median CH_2O ratio is 1.3. However, when removing extreme CCF data and in-cloud data points (identified as described in section 4.4.2) from the analysis, the correlation coefficient between measured and modeled CH_2O is essentially the same (0.46 versus 0.49), and the median calc/obs ratio is unchanged from the bulk value. This suggests that cloud effects, while clearly introducing

uncertainty, do not introduce bias into the comparison, and are insufficient to explain the large amount of scatter in agreement seen in Figure 7a.

5. CONCLUSIONS

A time dependent photochemical box model was used to evaluate fast photochemistry over the western Pacific and east Asian coast during the TRACE-P field campaign, using data obtained from two aircraft, NASA's DC8 and P3B. Critical model input precursor species such as O_3, CO, NO and NMHC, and critical physical input parameters were measured from both aircraft. Agreement between model predictions and observations of OH, HO_2, CH_2O, and NO_2 was examined.

The median calc/obs ratio for NO_2 on the DC8 indicated good agreement, with a value of 1.02, while analysis of NO_2 measured on the P3B aircraft revealed a model overprediction bias by a median of 25%. It has not been determined whether instrument interferences may contribute to this bias. The calc/obs ratios did not change when removing the extreme concentration data (NO_2 > 100 pptv) from the comparison. The r^2 correlation coefficient for the NO_2 calculations versus measurements was similar for the two aircraft, with values near 0.6 for concentrations below 100 pptv. About half of the measurements on the P3B and 58% of measurements on the DC8 were inside the range of expected instrument accuracy.

Model predictions of HO_2 measured on board the DC8 showed generally good agreement with measured values; 75% of the calculations fell within the instrument accuracy. The calc/obs ratio showed a consistent bias of 23% model overprediction throughout all altitudes. While the point to point correspondence was high, with r^2=0.88,

three subsets stood out from the preponderance of the data. Within the upper troposphere, stratospherically influenced air showed HO_2 calc/obs ratios that were quite low, with a median ratio of 0.63, versus a median ratio of 1.24 for the bulk of the data. A subset of data with high concentrations of NO (>135 pptv) likewise showed HO_2 calc/obs ratios lower than that for the bulk of the data, with a median of 0.97. A trend of decreasing HO_2 calc/obs ratio with higher NO is consistent with findings by *Faloona et al*. [2000] during the SUCCESS and SONEX field campaigns. Differences in dominant source and loss mechanisms between the subsets were identified, but uncertainties in rates of these reactions are not sufficient to explain the deviation in the HO_2 calc/obs ratio. At lower altitudes, data obtained within clouds showed a median calc/obs ratio of 1.55, substantially higher than the remainder of the data. This may be interpreted as observational evidence consistent with an uptake of HO_2 due to heterogeneous in-cloud loss. However, current simple theory for heterogeneous uptake of HO_2 overestimates the loss, with median decreases in predicted HO_2 of 70%. Heterogeneous loss of HO_2 to aerosol outside of clouds has a much smaller impact on HO_2 and these HO_2 measurements are not sensitive enough to independently verify the magnitude of this HO_2 loss.

OH is overpredicted in the middle troposphere by 60% for the DC8 and 40% for the P3B, with the overprediction increasing to 80% for the DC8 at the highest altitudes. Boundary layer and lower tropospheric OH calc/obs ratios decrease from middle tropospheric values for both aircraft, to 1.07 for the DC8 and to 0.7 for the P3B. For the DC8 data, 48% of OH model predictions were within the accuracy of the instrument, and for the P3B data, 85% of the predictions were within the stated instrument

precision. The HO_2/OH ratio at upper altitudes was underpredicted relative to measurements by about 23%, consistent with underpredictions of this ratio during previous field campaigns. The OH calc/obs ratio for the stratospherically influenced subset showed a median of 0.77, which is quite low relative to the majority of the data at upper altitudes (calc/obs = 1.81). Alternately, the OH calc/obs ratio was high for the high NO/high altitude subset (calc/obs = 2.01), suggesting an uncertainty related to the rate of HO_x recycling by NO.

Measurements of formaldehyde from the tunable diode laser absorption spectrometer were compared to model predictions. Similar to previous analyses, methanol observations were shown to increase predicted CH_2O by about 10% throughout the TRACE-P domain. The median model-measurement agreement is very good for data falling between the measurement LOD and 500 pptv, with a median calc/obs ratio of 1.02. However, the agreement is marked by large scatter (r^2 = 0.46). The general behavior of the model-to-measurement comparison differs distinctly across the spectrum of measured CH_2O mixing ratios, which is more clearly evident when smoothing the data. For concentrations greater than 500 pptv (about 7% of the data), the model increasingly underpredicts CH_2O with a median ratio of 0.66. It was determined that transport influences on CH_2O can be seen in the data, but affects only a very small portion (a few percent) of this data set. A test of the steady state assumption for CH_2O using a simulation of TRACE-P conditions by the Harvard GEOS-CHEM global model in place of the real atmosphere shows that this assumption is valid for the preponderance of the TRACE-P region. Results showed some evidence of transport impacts on CH_2O, but only to the small extent also suggested by the data.

For the CH_2O data between LOD and 500 pptv, the large scatter is likely due to a variety of causes, including finite measurement imprecision (2σ LOD ~ 60-80 pptv), uncertainties in the modeling approach (e.g., treatment of clouds), and uncertainties in CH_2O precursors, encompassing issues such as the limited availability of precursor measurements and also measurement issues such as unmeasured hydrocarbon species or uncertainties in measurements of precursors such as CH_3OOH. Some of these uncertainties were examined in this study. Specifically, it was found that CH_2O was quite sensitive to CH_3OOH, particularly at low altitudes and under low NO_x conditions. During TRACE-P, about 13% of the data below 2 km was potentially located within flight legs that showed oscillatory behavior of CH_2O as a result of limited availability of CH_3OOH. However, correlation between model predictions and measurements does not improve when limiting the analysis to only those points with measured CH_3OOH. This suggests that other uncertainties must play a dominant role. Similarly, while clouds are shown to introduce some uncertainty due to potential heterogeneous losses of CH_2O and the assumption of diurnal persistence of extreme local radiative deviations, those affected points were shown to introduce no bias to the model-to-measurement comparison. Further, the removal of those points had no impact on the calculated correlation between model predictions and measurements.

REFERENCES

Atkinson, R., D. L. Baulch, R. A. Cox, R. F. Hampson Jr., J.A. Kerr and J. Troe, Evaluated kinetic and photochemical data for atmospheric chemistry, Supplement IV, IUPAC subcommittee on gas kinetic data evaluation for atmospheric chemistry, *J. Phys. Chem. Ref. Data, 21,* 1125-1568, 1992.

Ayers, G.P., R.W. Gillett, H. Granek, C. de Serves, and R.A. Cox, Formaldehyde production in clean marine air, *Geophys. Res. Lett., 24*, 401-404, 1997.

Brune, W.H., P.S. Stevens, and J.H. Mather, Measuring OH and HO_2 in the troposphere by laser-induced fluorescence at low pressure, *J. Atmos.Sci., 52,* 3328-3336, 1995.

Brune, W.H., I.C. Faloona, D. Tan, A. J. Weinheimer, T. Campos, B.A. Ridley, S. A. Vay, J.E. Collins, G.W. Sachse, L. Jaeglé, and D.J. Jacob, Airborne in-situ OH and HO2 observations in the cloud-free troposphere and lower stratosphere during SUCCESS, *Geophys. Res. Lett., 25,* 1701-1704, 1998.

Cantrell, C., et al., Peroxy radical behavior during TRACE-P as measured aboard the NASA P-3B aircraft, *J. Geophys. Res.*, (in press), 2003.

Chameides, W.L., et al., Observed and model-calculated NO_2/NO ratios in tropospheric air sampled during the NASA GTE/CITE 2 field study, *J. Geophys. Res., 95,* 10,235-10,247, 1990.

Crawford, J. H., et al., Photostationary state analysis of the NO_2-NO system based on

airborne observations from the western and central North Pacific, *J. Geophys. Res., 101*, 2053-2072, 1996.

Crawford, J., D. Davis, J. Olson, G. Chen, S. Liu, G. Gregory, J. Barrick, G. Sachse, S.Sandholm, B. Heikes, H. Singh, and D. Blake, Assessment of upper tropospheric HO_x sources over the tropical Pacific based on NASA GTE/PEM data: Net effect on HO_x and other photochemical parameters, *J. Geophys. Res*., *104,* 16255-16273, 1999.

Davis, D.D., et al., Photostationary state analysis of the NO_2-NO system based on airborne observations from the subtropical/tropical North and South Atlantic, *J. Geophys. Res., 98,* 23501-23523, 1993.

DeMore W.B., S.P. Sander, D.M. Golden, R.F. Hampson, M.J. Kurylo, C.J. Howard, A.R. Ravishankara, C.E. Kolb and M.J. Molina, Chemical kinetics and photochemical data for use in stratospheric modeling, *JPL Publ., 97-4*, 1997.

Evans, M. et al., Understanding the emissions, processing, export and impact of Asian oxides of nitrogen, manuscript in preparation, to be submitted to J. Geophys. Res., 2003.

Faloona, I., D. Tan, W.H. Brune, L. Jaegle, D.J. Jacob, Y. Konda, M. Koike, R. Chatfield, R. Pueschel, G. Ferry, G. Sachse, S. Vay, B. Anderson, J. Hannon, and H. Fuelberg, Observations of HO_x and its relationship with NO_x in the upper troposphere during SONEX, *J. Geophys. Res*., *105 (D3),* 3771-3784, 2000.

Fried, A., Y.-N. Lee, G. Frost, B. Wert, B. Henry, J.R. Drummond, G. Hubler, and T.

Jobson, Airborne CH_2O measurements over the North Atlantic during the 1997 NARE campaign: instrument comparisons and distributions, *J. Geophys. Res*., *107*, doi: 10.1029/2000JD000260, 2002.

Fried, A., et al., Airborne tunable diode laser measurements of formaldehyde during TRACE-P: Distributions and box-model comparisons, *J. Geophys Res*., *108*, No. D20, 8798, doi:10.1029/2003JD003451, 2003a.

Fried, A., et al., Tunable diode laser measurements of formaldehyde during the TOPSE 2000 study: Distributions, trends, and model comparisons, *J. Geophys. Res*., *108*, 8365, doi: 10.1029/2002JD002208, 2003b.

Frost, G.J. et al., Comparisons of box model calculations and measurements of formaldehyde from the 1997 North Atlantic Regional Experiment*, J. Geophys. Res., 107*, doi:10.1029/2001JD000896, 2002.

Heikes, B.G., et al., Hydrogen peroxide and methylhydroperoxide distributions related to ozone and odd hydrogen over the North Pacific in the fall of 1991, *J. Geophys. Res*., *101*, 1891-1905, 1996.

Heikes, B., J. Snow, P. Egli, D.O'Sullivan, J. Crawford, J. Olson, G. Chen, D. Davis, N. Blake, and D. Blake, Formaldehyde over the central Pacific during PEM-Tropics B, *J. Geophys. Res., 106*, 32,717-32,731, 2001.

Jacob, D.J., B.G. Heikes, S.-M. Fan, J.A. Logan, D.L. Mauzerall, J.D. Bradshaw, H.B. Singh, G.L. Gregory, R.W. Talbot, D.R. Blake, and G.W. Sachse, Origin of ozone and NO_x in the tropical troposphere: a photochemical analysis of aircraft observations over the south Atlantic basin, *J. Geophys. Res*., *101*, 24,235-24,250, 1996.

Jacob, D.J., Heterogeneous chemistry and tropospheric ozone, *Atmos. Env*., *34*, 2131-2159, 2000.

Jacob, D.J., et al., J. Crawford, M. Kleb, V. Connors, R. Bendura, and J. Raper, The Transport and Chemical Evolution over the Pacific (TRACE-P) mission: Design, execution and overview of first results, *J. Geophys. Res*., (in press), 2003.

Jaeglé, L., et al., Observed OH and HO_2 in the upper troposphere suggest a major source from convective injection of peroxides, *Geophys. Res. Lett., 24*, 3181-3184, 1997.

Jaeglé, L., D.J. Jacob, W.H. Brune, D. Tan, I. Faloona, A.J. Weinheimer. B.A. Ridley, T.L. Campos, and G.W. Sachse, Sources of HOx and production of ozone in the upper troposphere over the United States, *Geophys. Res. Lett., 25*, 1705-1708, 1998.

Jaeglé, L., D.J. Jacob, W.H. Brune, I. Faloona, D. Tan, B.G. Heikes, Y. Kondo, G.W. Sachse, B. Anderson, G.L. Gregory, H.B. Singh, R. Pueschel, G. Ferry, D.R. Blake, and R.E. Shetter, Photochemistry of HO_x in the upper troposphere at northern midlatitudes, *J. Geophys. Res*., *105*, 3877-3892, 2000.

Lee, M., B.G. Heikes, D.J. Jacob, G. Sachse, and B. Anderson, Hydrogen peroxide, organic hydroperoxide, and formaldehyde as primary pollutants from biomass burning, *J. Geophys. Res*., *102*, 1301-1309, 1997.

Liu, S.C., M. Trainer, M.A. Carroll, G. Hubler, D.D. Montzka, R.B. Norton, B.A. Ridley, J.G. Walega, E.L. Atlas, B.G. Heikes, B.J. Huebert, and W. Warren, A study of the photochemistry and ozone budget during the Mauna Loa Observatory Experiment, J. Geophys. Res., *97*, 10,463-10,471, 1992.

Logan, J.A., M.J. Prather, S.C. Wofsy, and M.B. McElroy, Tropospheric chemistry: A global perspective, *J. Geophys. Res.*, *86*, 7210-7254, 1981.

Lowe, D.C. and U. Schmidt, Formaldehyde (HCHO) measurements in the nonurban atmosphere, *J. Geophy. Res.*, 88, 10,844-10,858, 1983.

Lurmann, F.W., A.C. Lloyd, and R. Atkinson, A chemical mechanism for use in long-range transport/acid deposition computer modeling, *J. Geophys. Res.*, *91*, 10905-10936, 1986.

Mauldin III, R.L., G.J. Frost, G. Chen, D.J. Tanner, A.S.H. Prevot, D.D.Davis and F.L. Eisele, OH measurements during the first aerosol characterization experiment (ACE 1): Observations and model comparisons, *J. Geophys. Res.*, *103*, 16713-16729, 1998.

Mauldin III, R.L., D.J. Tanner and F.L. Eisele, Measurements of OH during PEM Tropics, *J. Geophys. Res.*, *104*, 5817-5827, 1999.

Mauldin, R., C. Cantrell, M. Zondlo, E. Kosciuch, F. Eisele, G. Chen, D. Davis, R. Weber, J. Crawford, D. Blake, A. Bandy, and D. Thornton, Highlights of OH, H2SO4 and MSA measurements made aboard the NASA P-3B during TRACE-P, *J. Geophys. Res*. (in press), 2003.

McKeen, S.A., T. Gierczak, J.B. Burkholder, P.O. Wennberg, T.F. Hanisco, E.R. Keim, R.-S. Gao, S.C. Liu, A.R. Ravishankara, and D. W. Fahey, The photochemistry of acetone in the upper troposphere: A source of odd-hydrogen radicals, *Geophys. Res. Lett.*, *24*, 3177-3180, 1997.

Nakamura, K., Y. Kondo, M. Koike, N. Takegawa, K. Kita, G. Chen, J. Crawford,

R. Shetter, M. Avery, and J. Matsumoto, Measurements of NO2 by photolysis conversion technique during TRACE-P, *J. Geophys Res*., (in press), 2003.

Olson, J., et al., Seasonal differences in the photochemistry of the South Pacific: A comparison of observations and model results from PEM-Tropics A and B, *J. Geophys. Res*., *106*, 32749-32766, 2001.

Prather, M.J. and D.J. Jacob, A persistent imbalance in HOx and NOx photochemistry of the upper troposphere driven by deep tropical convection, *Geophys. Res. Lett., 24*, 3189-3192, 1997.

Ravishankara, A.R., E.J. Dunlean, M.A. Blitz, T.J. Dillon, D.E. Heard, M.J. Pilling, R.S. Strekowski, J.M. Nicovich, and P.H. Wine, Redetermination of the rate coefficient for the reaction of O(D-1) with N-2, *Geophys. Res. Lett*., *29*, Art. No. 1745, 2002

Sander, S.P., R.R. Friedl, W.B. DeMore, D.M. Golden, M.J. Kurylo, R.F. Hampson, R.E. Huie, G.K. Moortgat, A.R. Ravishankara, C.E. Kolb, and M.J. Molina, Chemical kinetics and photochemical data for use in stratospheric modeling: Supplement to Evaluation 12: Update of key reactions, *JPL Publ., 00-3*, 2000.

Sandholm, S., S. Smyth, R. Bai and J. Bradshaw, Recent and future improvements in two-photon laser-induced fluorescence NO measurement capabilities, *J. Geophys Res*., *102*, (D23), 28,651-28,661, 1997.

Shetter, R.E., and M. Müller, Photolysis frequency measurements using actinic flux spectroradiometery during the PEM-Tropics mission: Instrumentation description and some results, *J. Geophys. Res*., *104*, 5647-5661, 1999.

Sigsby, J.E., S. Gejada, W. Ray, J.M. Lang, and J.W. Duncan, Volatile organic

compound emissions from 46 in-use passenger cars, *Environ. Sci. Technol.*, *21*, 466-475, 1987.

Singh, H.B., M. Kanakidou, P.J. Crutzen, and D.J. Jacob, High concentrations and photochemical fate of oxygenated hydrocarbons in the global troposphere, *Nature*, *378*, 50-54, 1995.

Wagner, V., R. von Glascow, H. Fischer, and P.J. Crutzen, Are CH2O measurements in the marine boundary layer suitable for testing the current understanding of CH4 photooxidation?, *J. Geophys. Res.*, *107*, doi: 10.1029/2001JD000722, 2002.

Wang, Y., et al., Springtime photochemistry at northern mid and high latitudes, *J. Geophys. Res.*, (in press), 2002.

Weller, R.O., O. Schrems, A. Boddenberg, S. Gäb, and M. Gautrois, Meridional distribution of hydroperoxides and formaldehyde in the marine boundary layer of the Atlantic (48°N-25°S) measured during the Albatross campaign, J. Geophys. Res., *105*, 14,401-14,412, 2000.

Wennberg, P.O., et al., Hydrogen radicals, nitrogen radicals, and the production of O3 in the upper troposphere, *Science*, *279*, 49-53, 1998.

Zhou, X., Y.-N. Lee, L. Newman, X. Chen, and K. Mopper, Tropospheric formaldehyde concentration at the Mauna Loa Observatory during the Mauna Loa Observatory Photochemistry Experiment 2, *J. Geophys. Res.*, *101*, 14,711-14, 719, 1996.

1 Table 1. Statistics for subsets at altitudes > 7 km.

	Majority Points	**Stratospheric Points (O_3 > 120)**	**High NO Points (NO > 135)**
Number of Points	1499	112	169
Median Altitude (km)	9.2	10.0	10.1
Median Temperature (K)	237	226	229
Median SZA (degrees)	42	49	36
Median CCF(JO^1d)	1.23	1.05	1.25
Median HO_2 (pptv)	8.2	3.2	5.9
Median HO_2 calc/obs	1.24	0.63	0.97
Median OH calc/obs	1.64	0.77	2.01
Median O_3 (ppbv)	59	337	69
Median CO (ppbv)	102	44	118
Median H_2O (molecules cm^{-3})	$1.38x10^{15}$	$1.0x10^{14}$	$8.1x10^{14}$
Median C_2H_6 (pptv)	654	258	726
Median Acetone (pptv)	521	164	632
Median NO (pptv)	36	75	200
Median NO_2 (pptv)	12	41	40

2

Table 2. Selected Instantaneous HO_x Budget Terms for subsets at altitudes > 7 km

	Majority Points	**Stratospheric Points (O_3>120 pptv)**	**High NO Points (NO > 135 pptv)**
Model calculated production terms (10^3 molecules cm^{-3} s^{-1})			
O^1D+H_2O	32.3	5.30	34.0
Acetone photolysis assume yields=2 - 3	17.5 – 26.3	1.8 – 2.7	22.3 – 33.4
H_2O_2 photolysis	40.7	2.5	16.0
Model calculated loss Terms (10^3 molecules cm^{-3} s^{-1})			
$OH+HO_2$	41.9	3.7	53.9
HO_2+HO_2	67.4	2.5	21.6
Total for HOx-driven losses	*109.3*	*6.2*	*75.5*
$OH+NO_2$	2.3	4.5	17.8
HNO_4 cycling HO_x production (10^3 molecules cm^{-3} s^{-1})			
HNO_4 photolysis	2.7	3.2	6.3
HNO_4 thermal decomposition	3.4	0.9	0.9
HNO_4 cycling HO_x losses (10^3 molecules cm^{-3} s^{-1})			
HO_2+NO_2	13.1	13.6	29.4
HNO_4+OH	4.4	4.9	19.5

FIGURE CAPTIONS

Figure 1. Impact of oxygenates on prediction HO_x. Model results for a) HO_2 and b) OH are shown relative to a base run that neglects the impact of oxygenates. Boxes show the inner 50^{th} percentile of the ratios, and whiskers indicate the inner 90^{th} percentile. Data are shown as a function of altitude. Median values are shown by the center lines within the boxes. The impact from ketones (acetone and methyl ethyl ketone) is shown by the open boxes and the combined impact of ketones and alcohols (methyl and ethyl alcohol) is shown by the filled boxes.

Figure 2. Impact of peroxide constraints on predicted HO_x. See Figure 1 for definition of box and whiskers. Model predictions of a) HO_2 and b) OH are shown for a simulation with H_2O_2 and CH_3OOH constrained to observed values relative to a simulation where these peroxides are calculated. Ratios thus indicate the incidence and impact of non-equilibrium peroxide conditions on HO_x.

Figure 3. Calculated-to-observed ratio for NO_2 from the DC8 and P3B aircraft. See Figure 1 for definition of box and whiskers. Calculations of NO_2 are shown relative to observed values for the DC8 (open boxes) and the P3B (filled boxes) aircraft.

Figure 4. Comparison of calculated and observed OH on the DC8 and P3B aircraft. a) shows calculations of OH relative to observed values for the DC8 (open boxes) and the P3B (filled boxes) aircraft. See Figure 1 for definition of box and whiskers. Scatter plots of observed OH versus calculated OH are shown in b) for the DC8 aircraft and c) for the P3B aircraft.

Figure 5. Comparison of calculated and observed HO_2 on the DC8 aircraft. a) shows calculations of HO_2 relative to observed values for the DC8 aircraft. See Figure 1 for definition of box and whiskers. A scatter plot of observed HO_2 versus calculated HO_2 is shown in b) for the DC8 aircraft.

Figure 6. Subsets for HO_2 calculated-to-observed ratios on the DC8. a) shows the HO_2 calc/obs ratio versus altitude for the DC8 aircraft. Purple diamonds indicate data with O_3 greater than 120 ppbv (stratospheric data). Red triangles indicate data with NO greater than 135 pptv for altitudes above 7 km and gray triangles indicate high NO data for altitudes below 7 km. Green asterisks show data points that were identified as residing in clouds, using criteria described in the text. b) shows results from a test simulation including a heterogeneous loss of HO_2 to clouds and aerosols. Subsets are identified as in a).

Figure 7. Comparison of calculated and observed CH_2O from the DC8. a) shows a scatter plot of observed versus calculated CH_2O from the DC8. The agreement line is shown with a solid line. Note that data reported as negative do not appear on the logarithmic scale. b) shows a smoothed version of the observed CH_2O versus calculated values. The smoothed data was created by sorting the measurement-model pairs based on model concentration, and measurements were then smoothed using a 1% running average. Reported typical LOD value of 60 pptv is indicated with a dashed line, and the 500 pptv concentration level is also indicated with a dashed line. The agreement line is shown with the solid line.

Figure 8. Geographical locations of CH_2O measurements during TRACE-P. a) shows the latitude/longitude location of all CH_2O measurements by the laser spectrometer during TRACE-P, and b) shows those measurements greater than 500 pptv. c) indicates those points where CH_2O averages over hozontal flight legs are greater than 500 pptv. d) shows points within flight legs with CH_2O averages are greater than 500 pptv and where the calc/obs ratio is less than 0.7.

Figure 9. Box model/GEOS-CHEM CH_2O ratio as a function of altitude. Box model predictions of CH_2O are shown relative to that in the Harvard GEOS-CHEM model as a function of altitude. Input constraints for the box model simulations are retrieved from the GEOS-CHEM model output along simulated TRACE-P flight tracks..

Figure 10. Comparison of boxmodel predictions of CH_2O versus GEOS-CHEM and versus observational data from TRACE-P. a) The x-axis shows the upper 50^{th} percentile of concentrations of CH_2O in the GEOS-CHEM along simulated TRACE-P flight tracks and the y-axis shows the CH_2O box model/GEOS-CHEM ratio for those points. The solid line shows the median box model/GEOS-CHEM ratio for the entire data set. Numbers along the top portion of the figure indicated median ratios for the 10^{th} percentile segments along the concentration range. Open diamonds indicate the upper 5^{th} percentile of the GEOS-CHEM data. b) is the same display for observed CH_2O during TRACE-P and the corresponding box model predictions.

Figure 11. Geographical locations of CH_2O underpredictions of high concentrations from the GEOS-CHEM test simulation. Asterisks show points within simulated flight legs with CH_2O averages greater than 500 pptv and calc/obs ratios less than 0.7.

Figure 12. Impact of model constraint species on CH_2O. Relative differences in calculated versus constrained (observed) values for a) CH_3OOH, b) H_2O_2 and c) PAN are shown versus the associated relative difference in computed CH_2O. Values greater than 1 indicate a model overprediction of

the tested constraining species. Absolute differences (calculated minus observed constraint) are shown for d) CH_3OOH, e) H_2O_2 and f) PAN with the associated absolute difference in calculated CH_2O. Red symbols indicate where NO was greater than 50 pptv, and blue symbols indicate where NO was less than 5 pptv.

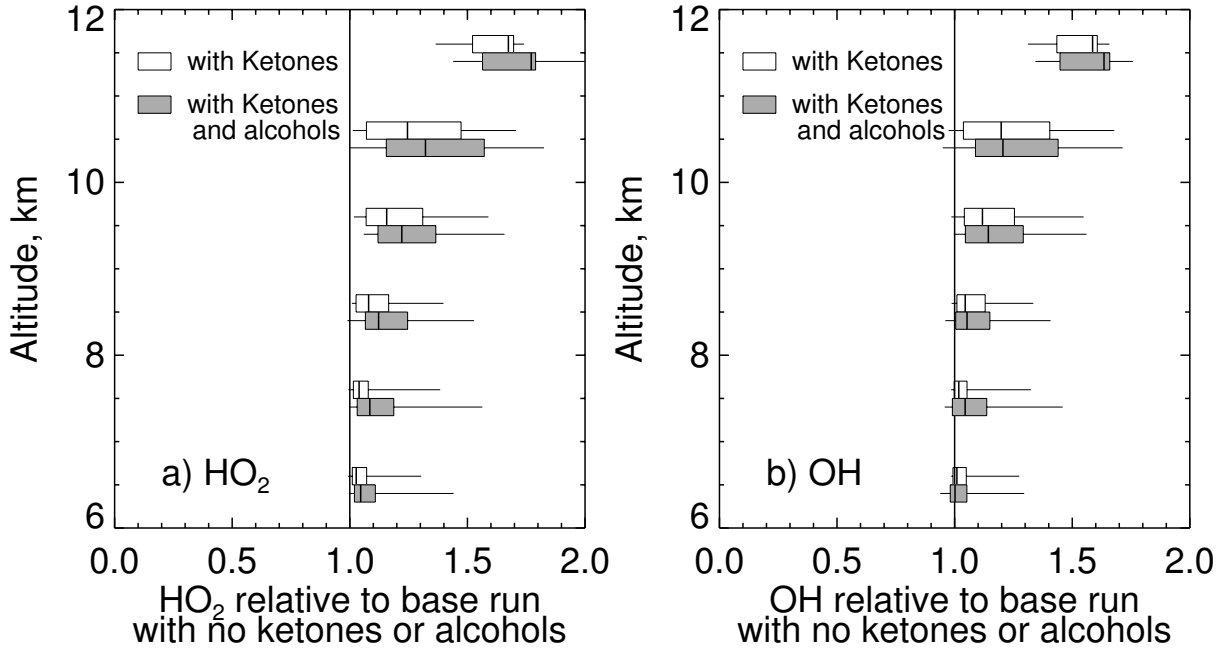

Figure 1. Impact of oxygenates on predicted HO_x.

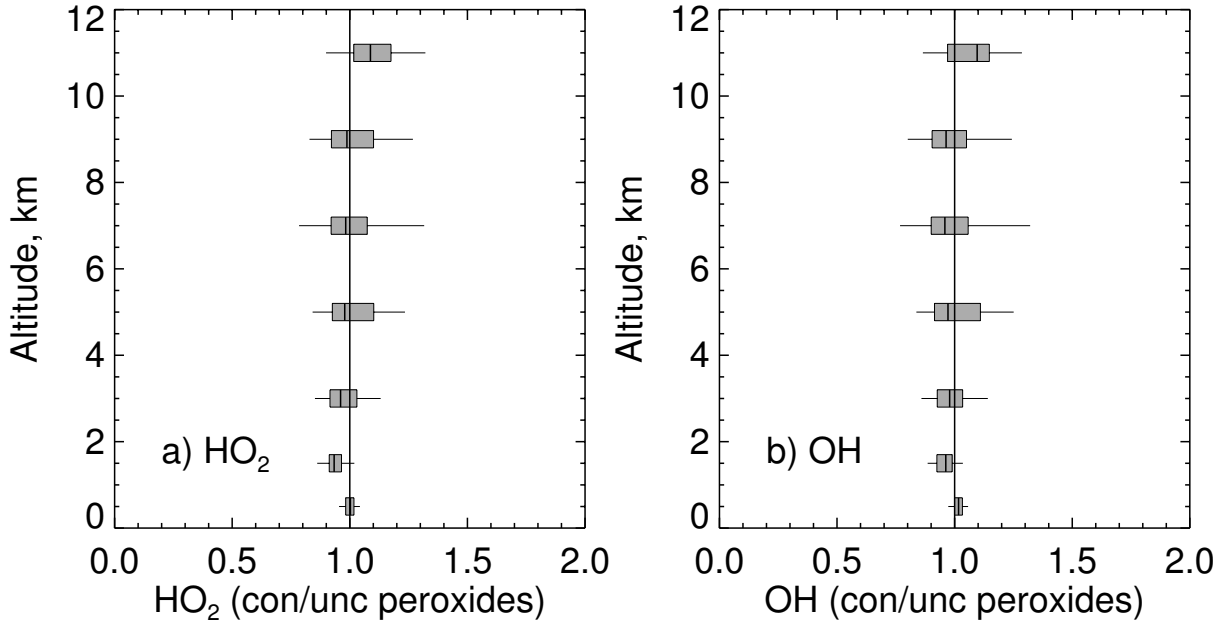

Figure 2. Impact of peroxide constraints on predicted HO_x.

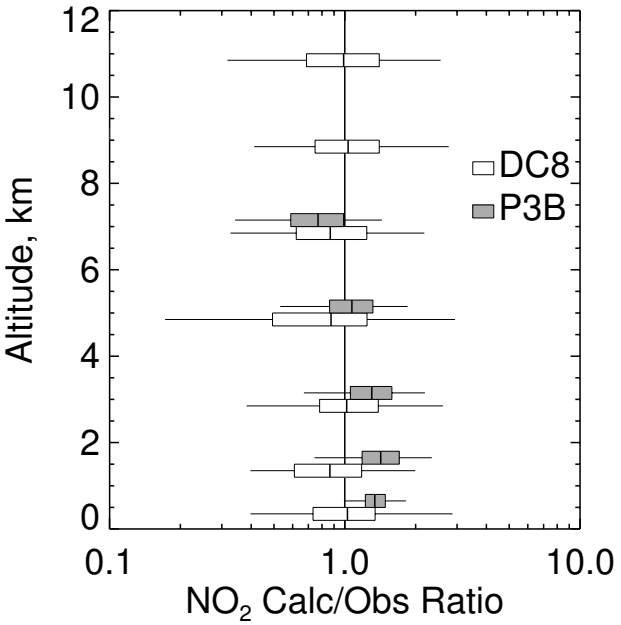

Figure 3. Calculated-to-observed ratio for NO_2 from the DC8 and P3B aircrafts

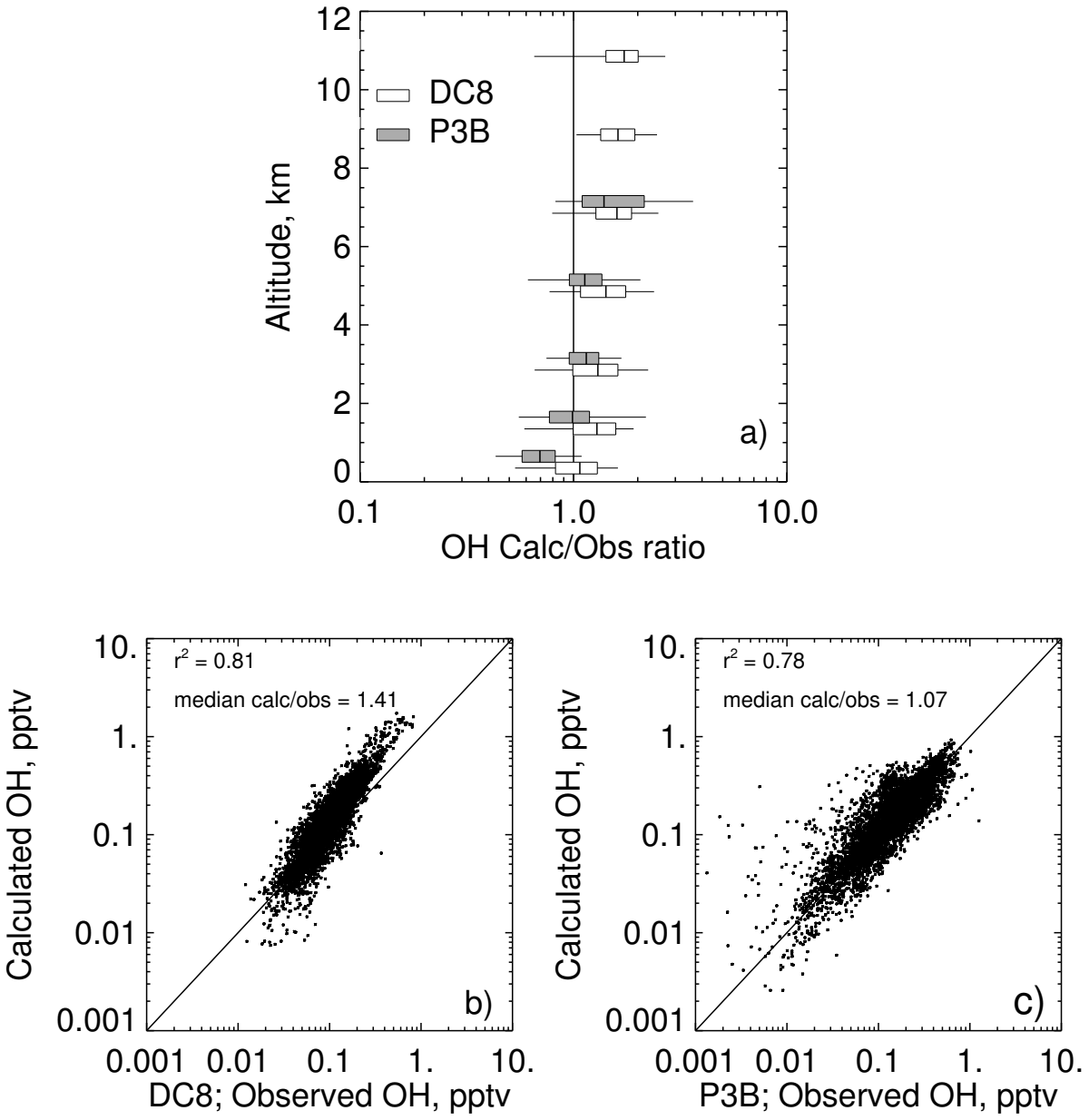

Figure 4. Comparison of calculated and observed OH on the DC8 and P3B aircraft.

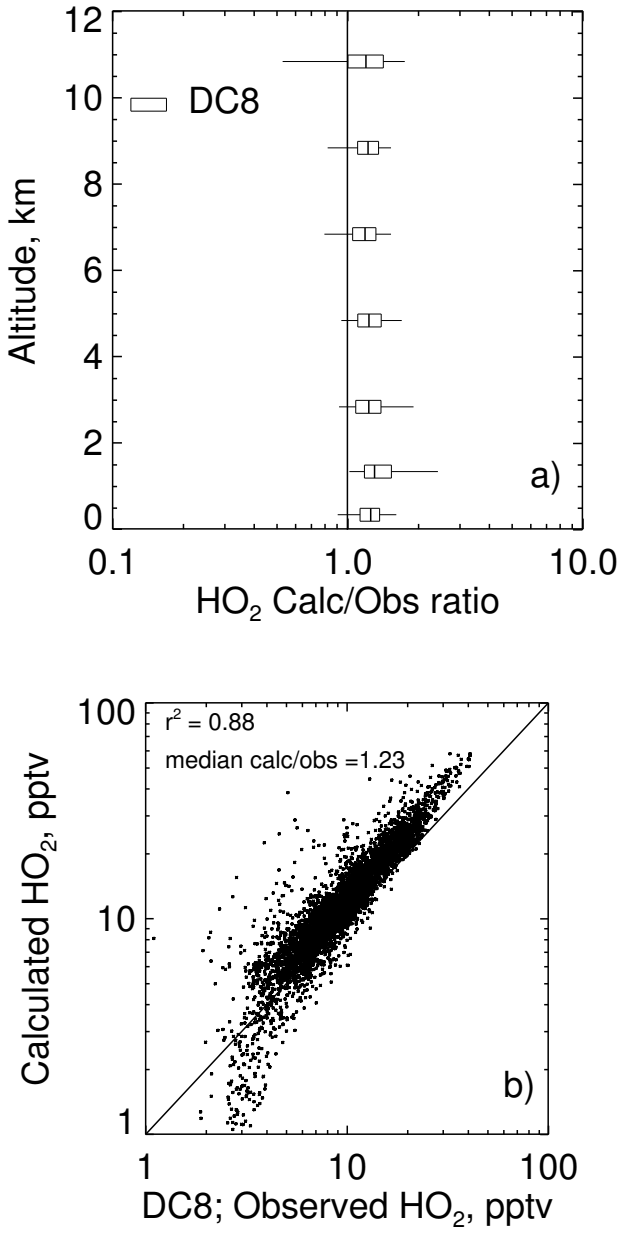

Figure 5. Comparison of calculated andobserved HO_2 on the DC8

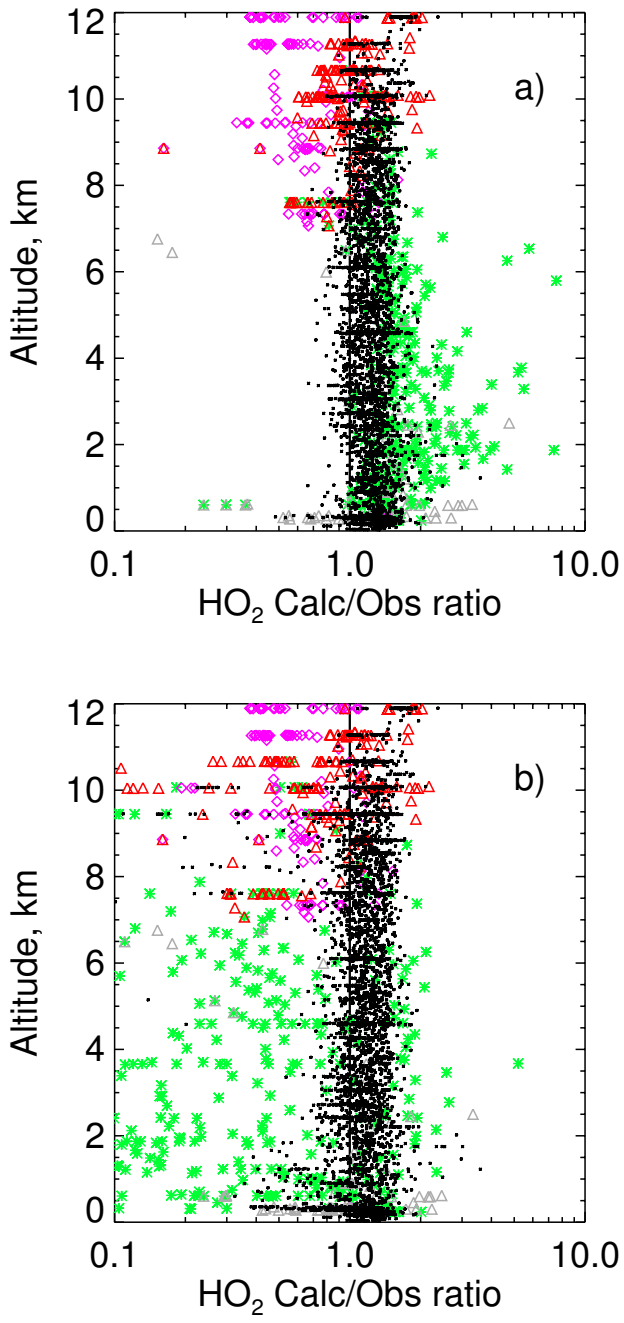

Figure 6. Subsets for HO_2 calculated-to-observed ratios on the DC8.

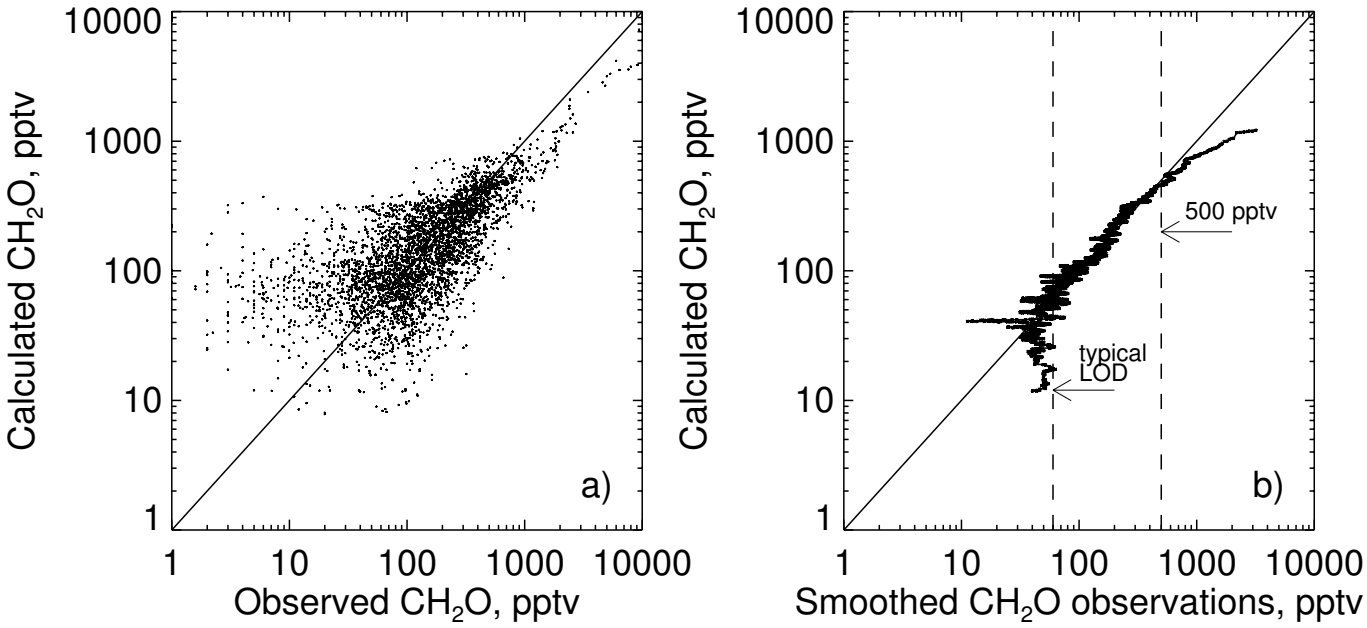

Figure 7. Comparison of calculated and observed CH_2O from the DC8.

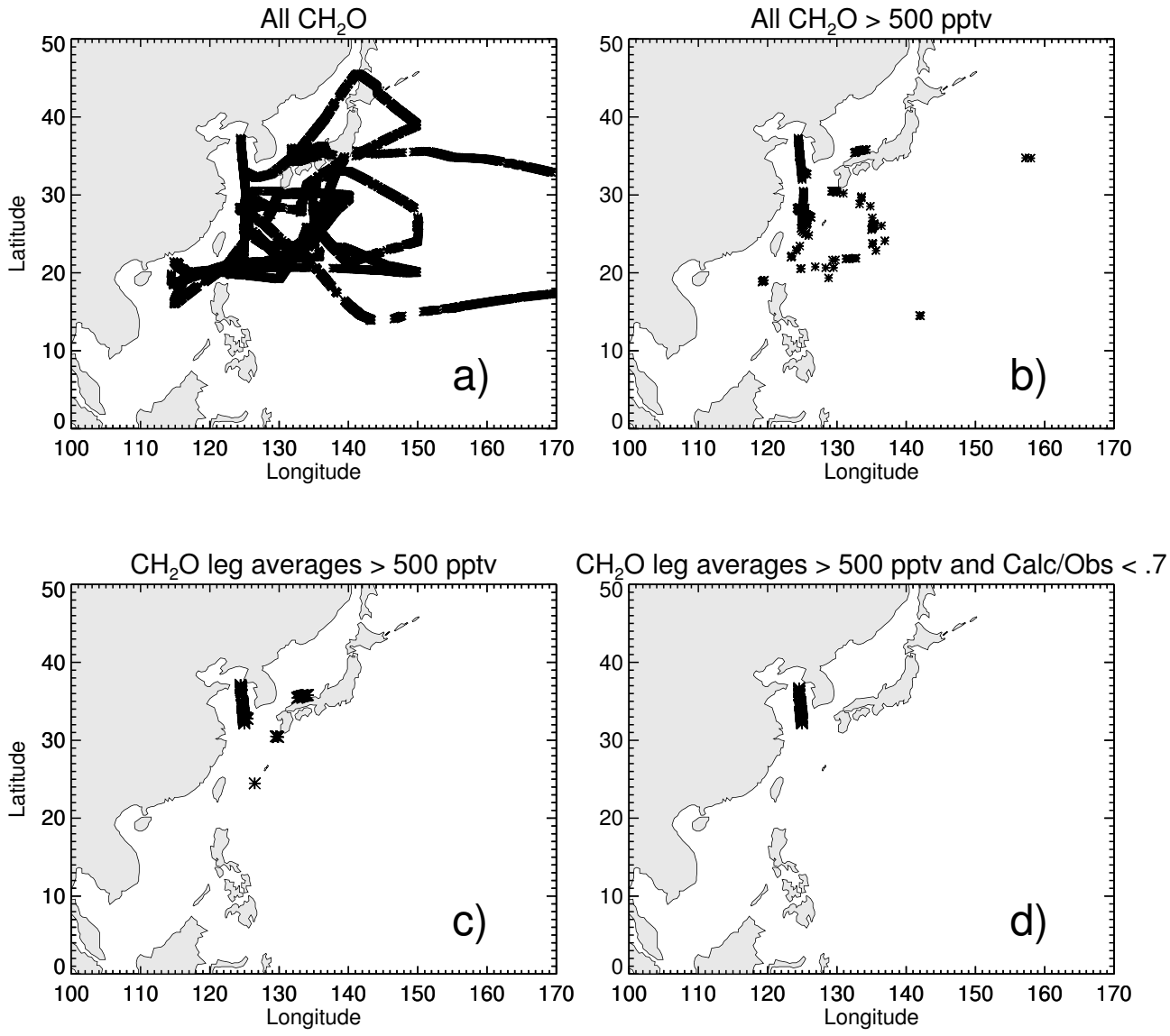

Figure 8. Geographical locations of CH_2O measurements during TRACE P

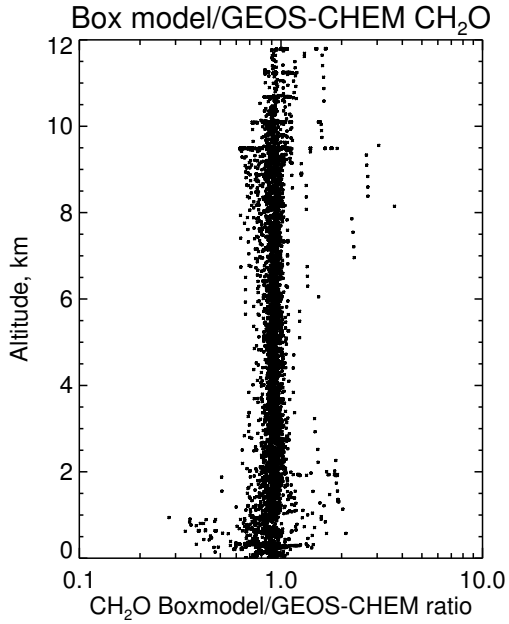

Figure 9. Box model/GEOS-CHEM CH_2O ratio as a function of altitude.

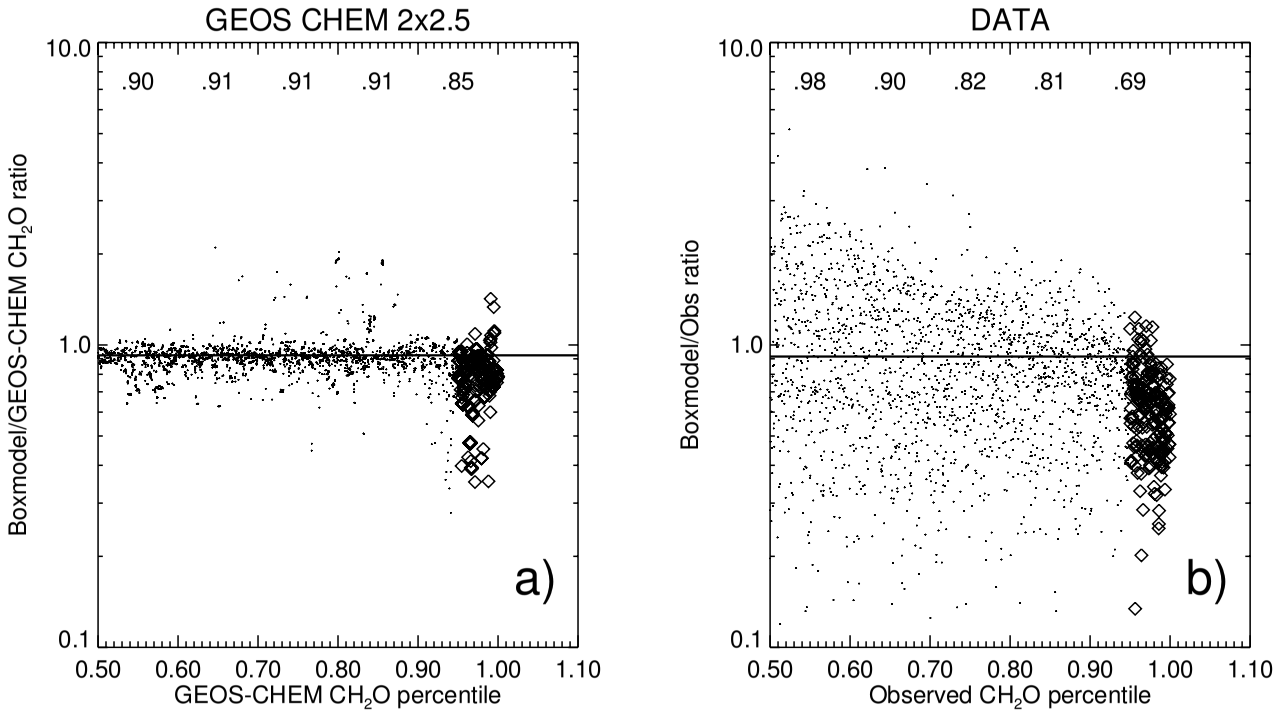

Figure 10. Comparison of boxmodel predictions of CH_2O versus GEOS CHEM and versus real data.

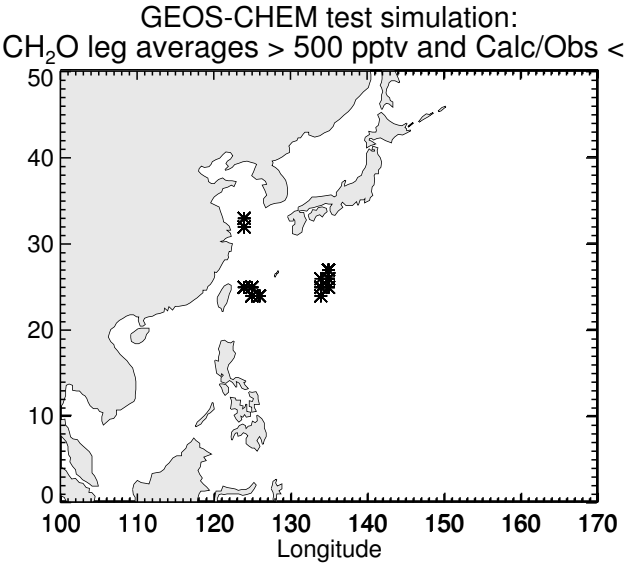

Figure 11. Geographical locations of CH_2O underpredictions of high concentrations from the GEOS-CHEM test simulation.

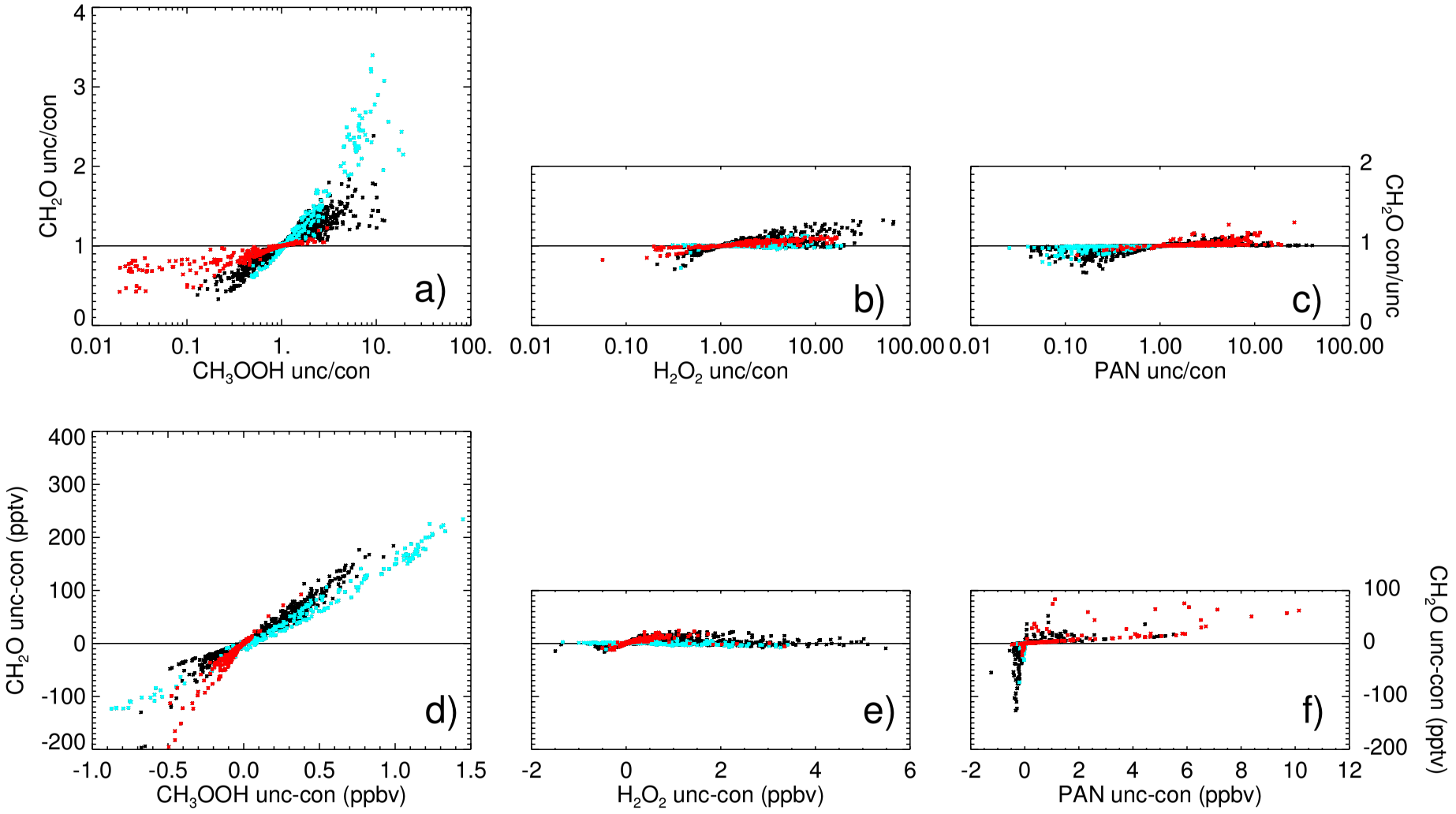

Figure 12. Impact of model constraint species on CH_2O